CORE
Metadata, citation and similar papers at core.ac.uk
Provided by Directory of Open Access Journals

Journal of the Serbian Chemical Society
JSCS-info@shd.org.rs • www.shd.org.rs/JSCS
J. Serb. Chem. Soc. *77* (11) 1483–1528 (2012)
JSCS–4367
UDC 546.46:66.087.3+533.9:519.6+54
Review

REVIEW

A multidisciplinary study on magnesium

RADOMIR RANKOVIĆ[1#], STEVAN STOJADINOVIĆ[2], MIRJANA SARVAN[2], BEĆKO KASALICA[2], MARIJA KRMAR[1], JELENA RADIĆ-PERIĆ[1#] and MILJENKO PERIĆ[1*#]

[1]Faculty of Physical Chemistry, University of Belgrade, Studentski trg 12–16, P.O. Box 47, 11158 Belgrade Serbia and [2]Faculty of Physics, University of Belgrade, Studentski trg 12–16, 11158 Belgrade Serbia

(Received 12 September, revised 10 October 2012)

Abstract: During plasma electrolytic oxidation of a magnesium alloy (96 % Mg, 3 % Al and 1 % Zn), a luminescence spectrum in the wave number range between 19950 and 20400 cm^{-1} was obtained. The broad peak with a clearly pronounced structure was assigned to the v′–v″ = 0 sequence of the $B^1\Sigma^+ \rightarrow X^1\Sigma^+$ electronic transition of MgO. Quantum-mechanical perturbative approach was applied to extract the form of the potential energy curves for the electronic states involved in the observed spectrum, from the positions of the spectral bands. These potential curves, combined with the results of quantum-chemical calculations of the electric transition moment, were employed in subsequent variational calculations to obtain the Franck–Condon factors and transition moments for the observed vibrational transitions. Comparing the results of these calculations with the measured intensity distribution within the spectrum, the relative population of the upper electronic state vibration levels was derived. This enabled the plasma temperature to be estimated. Additionally, the temperature was determined by analysis of the recorded $A^2\Sigma^+$ (v′ = 0) – $X^2\Pi$ (v″ = 0) emission spectrum of OH. The composition of the plasma containing magnesium, oxygen, and hydrogen under the assumption of a local thermal equilibrium was calculated in the temperature range up to 12000 K and for pressures of 10^5, 10^6, 10^7, and 10^8 Pa, in order to explain the appearance of the observed spectral features and to contribute to the elucidation of processes occurring during the electrolytic oxidation of Mg.

Keywords: magnesium alloy; plasma electrolytic oxidation; galvanoluminescence; $B^1\Sigma^+ \rightarrow X^1\Sigma^+$ electronic transition of MgO; perturbative and variational quantum-mechanical methods; *ab initio* quantum-chemical calculations; computation of plasma composition.

* Corresponding author. E-mail: peric@ffh.bg.ac.rs
# Serbian Chemical Society member.
doi: 10.2298/JSC120912105R

2012 Copyright (CC) SCS

CONTENTS

1. INTRODUCTION

The usual form of a review paper is such that the author picks up some research field, sometimes a particular method, and reports briefly about all the systems which have been investigated in/with it. In the other words, he writes nothing about everything (but “everything” only for those who are working in the same field, or using the same method). In the present review, we take the opposite point of view. We consider a particular element, magnesium, even only a molecule that involves it, MgO, eventually solely a spectral band sequence of this molecule, and show all that we were able and/or forced to do on it in order to make an infinitesimal progress in our knowledge of some particular properties of this element. Figuratively speaking again, we write everything about nothing.

2. PHYSICS CHEMISTRY, MATERIAL SCIENCE

Magnesium is one of the most abundant elements on the Earth, but also, as is nowadays believed, in the whole universe[1–3] (see Supplement A). Elemental

2012 Copyright (CC) SCS

magnesium is a fairly strong, silvery-white, light-weight (two thirds the density of aluminium) alkaline earth metal. It is highly reactive and thus not found naturally on Earth. However, when once produced, it is coated with a thin layer of oxide (passivation), which partly masks this reactivity. It is mainly obtained by electrolysis of magnesium salts extracted from brine. Magnesium is highly flammable when molten or in powder or ribbon form. It burns in air with a characteristic brilliant white light, which includes strong ultraviolet radiation. The flame temperature of Mg and Mg alloys can reach over 3000 °C. Once ignited, it is difficult to extinguish, being able to burn in nitrogen (forming magnesium nitride), carbon dioxide (forming magnesium oxide) and water (forming magnesium oxide). Commercially, the main use for the metal is as an alloying agent to make aluminium–magnesium alloys, called "magna(e)lium". These alloys are useful for their relative lightness and strength. An important application field of magnesium is electronic devices. Owing to its low weight, and good mechanical and electrical properties, magnesium is widely used for the manufacture of automotive and truck components, mobile phones, laptop and tablet computers, cameras, and other electronic components. Due to important interactions between phosphate and magnesium ions, magnesium is essential to the basic nucleic acid chemistry of life, and thus to all cells of all known living organisms. Over 300 enzymes require the presence of magnesium ions for their catalytic action. Plants have an additional use for magnesium in that chlorophylls are magnesium-centred porphyrins. Magnesium compounds are typically white crystals. Most are soluble in water. They, primarily magnesium oxide (MgO), are used as refractory materials in furnace linings for the production of iron, steel, non-ferrous metals, glass and cement, and also in the agricultural, chemical, and construction industries.

3. SPECTROSCOPY

3.1. Transitions

The intensity of the transition between two molecular states described by the wave functions Ψ'' and Ψ' is proportional to the square of the transition moment (TM) defined as:[4,5]

$$R^{',''} = \int \Psi'^{*} A \Psi'' \mathrm{d}\tau \tag{1}$$

where A is the operator that determines the mechanism of the transition. In the most important case of "optical" transitions, considered here, A is the (vector) dipole operator, $\vec{\mu}$, defined by:

$$\vec{\mu} = \sum_i q_i \vec{r}_i \tag{2}$$

where q_i is the charge and $\vec{r}_i$ is the radius vector of the i-th particle. The sum runs over all charged particles (electrons and nuclei). The proportionally factor

2012 Copyright (CC) SCS

between the intensity of an transition and the square of the TM involves, beside natural constants and statistical weights, in the case of absorption, the energy difference, ΔE, between the levels in question, and at emission ΔE^4. Assuming the general case, when the two energy levels in question belong to different electronic (e), vibrational (v), rotational (r), and spin states, Eq. (1) can be written as:

$$\vec{R}^{\prime,\prime\prime} = \int\int\int\int \Psi^{\prime *}(\mathrm{e,v,r,s})\vec{\mu}\Psi^{\prime\prime}(\mathrm{e,v,r,s})\mathrm{d}\tau_\mathrm{e}\mathrm{d}\tau_\mathrm{v}\mathrm{d}\tau_\mathrm{r}\mathrm{d}\tau_\mathrm{s} \tag{3}$$

The total wave functions, Ψ'' and Ψ', are usually (in the framework of the non-relativistic, Born–Oppenheimer (B–O), rigid rotator/infinitesimal vibrator approximations) assumed as products of the partial wave functions describing individual degrees of freedom, *i.e*. in the form:

$$\Psi(\mathrm{e,v,r,s}) = \psi_\mathrm{e}\psi_\mathrm{v}\psi_\mathrm{r}\psi_\mathrm{s} \tag{4}$$

If only "allowed" transitions are of interest, the spin variables can be excluded from consideration since in this case transitions are only possible when both states in question have the same spin function. The problem now is that the rotation functions are defined in a space-fixed coordinate system, while the electronic and vibrational functions are naturally expressed in a moving coordinate system tied to the molecule. Thus, one has to start with the expression for the components of TM, μ_F ($F = X, Y, Z$), along the axes of the space-fixed frame:

$$R_F^{\prime,\prime\prime} = \int\int\int \psi_\mathrm{r}^{*\prime}\psi_\mathrm{v}^{*\prime}\psi_\mathrm{e}^{*\prime}\mu_F\psi_\mathrm{e}^{\prime\prime}\psi_\mathrm{v}^{\prime\prime}\psi_\mathrm{r}^{\prime\prime}\mathrm{d}\tau_\mathrm{e}\mathrm{d}\tau_\mathrm{v}\mathrm{d}\tau_\mathrm{r} \tag{5}$$

and then transform some of the quantities to the molecule-fixed frame, x, y, z. The components of the dipole operator transform as:

$$\mu_F = \sum_g \lambda_{Fg}\mu_g \tag{6}$$

where $g = x$, y or z, and λ_{Fg} are the elements of the transformation matrix that involves sin and cos functions of two eulerian angles ϕ and θ. Since (only) the rotation functions depend on the eulerian angles (and only on them), Eq. (5) can be transformed into:

$$R_F^{\prime,\prime\prime} = \sum_g \int \psi_\mathrm{r}^{*\prime}\lambda_{Fg}\psi_\mathrm{r}^{\prime\prime}\mathrm{d}\tau_\mathrm{r}\left[\int \psi_\mathrm{v}^{*\prime}\left(\int \psi_\mathrm{e}^{*\prime}\mu_g\psi_\mathrm{e}^{\prime\prime}\mathrm{d}\tau_\mathrm{e}\right)\psi_\mathrm{v}^{\prime\prime}\mathrm{d}\tau_\mathrm{v}\right] \tag{7}$$

The expression in parentheses:

$$\int \psi_\mathrm{e}^{*\prime}\mu_g\psi_\mathrm{e}^{\prime\prime}\mathrm{d}\tau_\mathrm{e} \equiv R_g^{\prime,\prime\prime} \tag{8}$$

is the g-component of the "electric transition moment" (actually, in this context it would be more logical to call this quantity the electronic TM, to stress that the integration is carried out only with respect to the electronic coordinates; however, most authors prefer the term "electric", to distinguish this quantity from, *e.g*., the

2012 Copyright (CC) SCS

magnetic TM). The electric TM represents a generalization of the usual electric dipole moment (obtained from Eq. (8) when $\Psi_{e'} = \Psi_{e''}$) and, unlike the latter, it can, even in diatomic molecules, have both parallel and perpendicular components with respect to the molecular axis. This quantity is a function of the bond length, r (*i.e.*, of the vibrational coordinate), and can thus be represented by a Taylor expansion:

$$R_g^{',''} = \left(R_g^{',''}\right)_{r=r_e} + \left(\frac{\mathrm{d}R_g^{',''}}{\mathrm{d}r}\right)_{r=r_e} \left(r - r_e\right) + \ldots \tag{9}$$

where r_e is the equilibrium bond length. Inserting Eq. (9) into Eq. (7), one obtains:

$$R_F^{',''} = \sum_g \int \psi_{r'}^* \lambda_{Fg} \psi_{r''} \mathrm{d}\tau_r \times$$
$$\times \left[\left(R_g^{',''}\right)_{r=r_e} \int \psi_{v'}^* \psi_{v''} \mathrm{d}\tau_v + \left(\frac{\mathrm{d}R_g^{',''}}{\mathrm{d}r}\right)_{r=r_e} \int \psi_{v'}^* \left(r - r_e\right) \psi_{v''} \mathrm{d}\tau_v + \ldots \right] \tag{10}$$

With help of Formula (10), all the selection rules for optical transitions in diatomic molecules can be discussed. Since electronic transitions are dealt with in the present study, pure rotation and vibration–rotation transitions are discussed very briefly.

i) Pure rotation spectra, $e' = e'' \equiv e$, v' = v'' ≡ v, $r' \neq r''$. In this case, $\int \psi_v^* \psi_v \mathrm{d}\tau_v = 1$, and in the harmonic approximation $\int \psi_v^* \left(r - r_e\right) \psi_v \mathrm{d}\tau_v = 0$. The electric TM becomes then the dipole moment of the molecule that, due to axial symmetry of diatomic molecules, always lies along the internuclear axis (z). Equation (10) reduces then to:

$$R_F^{',''} = \left(R_z^e\right)_{r=r_e} \sum_g \int \psi_{r'}^* \lambda_{Fg} \psi_{r''} \mathrm{d}\tau_r \tag{11}$$

A rotation spectrum can thus appear only if the molecule considered has a non-vanishing dipole moment. Such are heteronuclear, but not homonuclear diatomics. The situation concerning the transition rules is not changed even if one goes beyond the harmonic approximation; for a homonuclear diatomic molecule $\mathrm{d}R_g^e / \mathrm{d}r$, as well as all higher derivatives equal zero. A pure rotation spectrum consists of a number of nearly equidistant lines with the spacing in the order of magnitude of typically 10 cm^{-1}, which form a molecular band.

ii) Vibration–rotation spectra, $e' = e'' \equiv e$, v' ≠ v''. In this case, $\int \psi_{v'}^* \psi_{v''} \mathrm{d}\tau_v = 0$, and Eq. (10) reduces to:

2012 Copyright (CC) SCS

$$R_F^{',''} = \left(\frac{\mathrm{d}R_Z^{\mathrm{e}}}{\mathrm{d}r} \right)_{r=r_{\mathrm{e}}} \sum_g \int \psi_{\mathrm{r}'}^* \lambda_{Fg} \psi_{\mathrm{r}''} \mathrm{d}\tau_{\mathrm{r}} \int \psi_{\mathrm{v}'}^* \left(r - r_{\mathrm{e}} \right) \psi_{\mathrm{v}''} d\tau_{\mathrm{v}} + \ldots \qquad (12)$$

Since Expression (12) equals zero when there is no change in the dipole moment with variation of the bond length, only heteronuclear diatomics can have a vibration–rotation spectra. In the harmonic approximation, the second integral implies the selection rule v′ – v″ = ±1. In higher approximations, "overtones" are possible, corresponding to the selection rule v′ – v″ = ±2, ±3, … but they are normally of low intensity. The rotation selection rules are determined by the first integral, and they are the same as for pure rotational transitions. Each vibrational transition is accompanied by a number of rotational ones. Owing the above selection rules for vibrational transitions, a vibration–rotation spectrum is usually similar to a pure rotational one, the most prominent difference being that the former appears in the near and the latter in the far infrared region.

iii) Electronic transitions, $e' \neq e''$. In the first Franck–Condon (F–C) approximation, the second term in the square parentheses on the right-hand side of Eq. (10) can be neglected:

$$R_F^{',''} \cong \left(R_g^{',''} \right)_{r=r_0} \sum_g \int \psi_{\mathrm{r}'}^* \lambda_{Fg} \psi_{\mathrm{r}''} \mathrm{d}\tau_{\mathrm{r}} \int \psi_{\mathrm{v}'}^* \psi_{\mathrm{v}''} d\tau_{\mathrm{v}} \qquad (13)$$

Instead of the dipole moment, as in Eqs. (11) and (12), one now has the electric TM (see. Eq. (8)), which also in homonuclear diatomics can be non-zero. It will be non-vanishing if the product of the irreducible representations of the electronic wave functions equals the irreducible representation of the *x*-, *y*-, or *z*-components of the dipole operator. In the case of heteronuclear diatomics, the *z*-component of this operator belongs to the Σ^+, and *x*- and *y*-components build together a basis for the Π irreducible representation of the point group $C_{\infty v}$. This results in the selection rule $\Delta\Lambda = 0, \pm 1$, where $\Lambda = 0$ (Σ^+ or Σ^- electronic state), 1 (Π state), 2 (Δ state), *etc.*, is the projection of the electronic angular momentum along the internuclear axis. An additional selection rule is that the transitions $\Sigma^+ \leftrightarrow \Sigma^+$ and $\Sigma^- \leftrightarrow \Sigma^-$ are allowed, while the transitions $\Sigma^+ \leftrightarrow \Sigma^-$ are forbidden. In the case of homonuclear diatomics, the *z*-component of this operator belongs to a Σ_u^+, and the *x*- and *y*-components to a Π_u irreducible representation of the point group $D_{\infty \mathrm{h}}$. This yields the additional selection rule that an electronic transition is allowed only if one of the combining states has *g* and the other *u* symmetry. All the mentioned selection rules (as well as $\Delta S = 0$, where *S* is the total electronic spin of the molecule) are valid within the framework of the non-relativistic and B–O approximation.

The square of the second integral in Eq. (13), representing the overlap of the vibrational wave functions of the combining state:

2012 Copyright (CC) SCS

$$FC \equiv \left[\int \psi_{v'}^{*} \psi_{v''} \mathrm{d}\tau_{v} \right]^{2} \quad (14)$$

is called the Franck–Condon factor (FCF). Unlike the case of pure vibration(––rotation) spectra, it is not subject to any selection rules. Very often, the electronic spectra are recorded using instruments of relatively low resolution, such that it is not possible to clearly identify the rotational structure of bands but only the positions of their maxima ("heads"). The magnitudes of the FCFs determine the intensity distribution within a band system, which consists of transitions between different vibrational levels of two electronic states. The most prominent features in spectral systems are band progressions (characterized in absorption by a fixed vibrational quantum number v″ of the lower electronic state, and variable quantum number v′ in the excited state, and fixed v′ and variable v″ in emission) and sequences (v′ – v″ = const.). If the equilibrium bond lengths and vibrational frequencies are similar in both electronic states, the most intense band in an experimentally recorded spectrum corresponds to the transition v′ – v″ = 0. A long progression with the maximum at a quite large value of $|v' - v''|$ indicates that the equilibrium bond lengths in the combining electronic states are appreciably different. Electronic spectra appear in the visible and ultraviolet region. While the band heads in a progression are separated from one another by several hundreds to a few thousand cm^{-1} (corresponding to the wave numbers of the vibrational frequencies), the separation of the bands in a sequence is usually between several tens and several hundreds cm^{-1}, reflecting the difference in the values of vibrational frequencies in the two electronic states in question.

The F–C approximation is thus mathematically based on the assumption that the electric transition moment is a constant quantity. In terms of naive quantum mechanics or classical physics, if one considers, for example, absorption, it can be interpreted such that the electronic transition occurs so quickly that the nuclei remain after the jump from the lower into upper state in the same position where they were at the beginning of the electron jump. This picture is quite compatible with that lying behind the B–O approximation. More sophisticatedly speaking, the transition is most probable to a vibrational level the wave function of which has the largest overlap with that of the starting vibrational level ("vertical" transition).

Going beyond the F–C approximation, the dependence of the electric TM on the internuclear distance, as indicated by the second term on the right-hand side of Eq. (10), has to be taken into account. In a diatomic molecule, this only quantitatively influences the transition probabilities and can make the transition not strictly "vertical". However, in the case of a polyatomic species, the consequences of the incorporation of this term into the treatment can be dramatic; it can happen, namely, that the value of the electric TM at the equilibrium geometry vanishes, but not its (first) derivative with respect to a particular non-to-

2012 Copyright (CC) SCS

tally symmetric vibrational coordinate (the unique vibrational coordinate in diatomics is totally symmetric). In this case, a transition forbidden in the F–C approximation becomes "vibronically induced".

The intensity of the spectral band appearing as a consequence of the emission transition between the vibrational level v′ of the electronic state e′ and the vibrational level v″ of the electronic e″ is determined by the formula:

$$I_{e'v',e''v''} \propto N_{v'}\left(E_{v'e'} - E_{e''v''}\right)^4 \left|\vec{R}^{e'v',e''v''}\right|^2 e^{-\frac{E_{v'e'}-E_{e''v''}}{kT}} \equiv$$
$$\equiv N_{v'}\left(E_{v'e'} - E_{e''v''}\right)^4 (TM)_{e'v',e''v''} e^{-\frac{E_{v'e'}-E_{e''v''}}{kT}} \quad (15)$$

where $E_{v'e'}$ and $E_{v''e''}$ are the energies of these two states, $R^{e'v',e''v''}$ is the vibrational transition moment, $N_{v'}$ is the number of molecules in the upper state, k is the Boltzmann constant and T temperature. The notation $(TM)_{e'v',e''v''} = \left|R^{e'v',e''v''}\right|^2$ for the square of the vibrational TM is introduced. Since the energy differences between all transitions to be handled in the present study, namely the members of the v′ – v″ = 0 sequence, (0–0), (1–1),… are negligibly small compared to the energy of the electronic transition, the quantity $E_{v'e'} - E_{v''e''}$ can be, in this context, handled as constant and then the number of the molecules in the upper state is:

$$N_{v'} \propto \frac{I_{e'v',e''v''}}{(TM)_{e'v',e''v''}} \quad (16)$$

In the F–C approximation, it is assumed that the electric TM is constant, and in this case the formula (16) reduces to

$$N_{v'} \propto \frac{I_{e'v',e''v''}}{(FCF)_{e'v',e''v''}} \quad (17)$$

where $(FCF)_{e'v',e''v''}$ is the F–C factor for the transition considered.

Assuming a local thermal equilibrium of the system, the ratio of the number of molecules $N_{e'v'}$ in the vibrational state v′ and in the lowest vibrational state v′ = 0 of the same electronic species, $N_{e'0}$, is determined by:

$$\frac{N_{e'v'}}{N_{e'0}} = e^{-\frac{E_{e'v'}-E_{e'0}}{kT}} \quad (18)$$

i.e.,:

$$\ln\left(\frac{N_{e'v'}}{N_{e'0}}\right) = -\frac{E_{e'v'} - E_{e'0}}{kT} \quad (19)$$

Combining the Formulae (16), (17) and (19), for the sequence v′ = v″, one obtains:

2012 Copyright (CC) SCS

$$\ln\left[\frac{\frac{I_{e'v,e''v}}{(TM)_{e'v',e''v''}}}{\frac{I_{e'0,e''0}}{(TM)_{e'0,v'0}}}\right]=-\left(\frac{E_{e'v'}-E_{e'0}}{k}\right)\frac{1}{T} \quad (20)$$

and

$$\ln\left[\frac{\frac{I_{e'v,e''v}}{(FCF)_{e'v,e''v}}}{\frac{I_{e'0,e''0}}{(FCF)_{e'0,e''0}}}\right]=-\left(\frac{E_{e'v'}-E_{e'0}}{k}\right)\frac{1}{T} \quad (21)$$

The Formulae (20) and/or (21) will be used later to determine the plasma temperature.

3.2. Vibrational structure of spectra

Experimentally derived vibrational energy levels of an electronic state are usually represented by the formula:[4]

$$E_v \equiv T_e hc + G(v)hc = \\ = T_e hc + hc\omega_e\left(v+\frac{1}{2}\right) - hc\omega_e x_e\left(v+\frac{1}{2}\right)^2 + hc\omega_e y_e\left(v+\frac{1}{2}\right)^3 + \ldots \quad (22)$$

where $G(v)$ are the corresponding term values (in cm^{-1}). In Eq. (22), T_e is the electronic term value; for the ground electronic state $T_e = 0$. Herzberg[4] called (as many people working in molecular spectroscopy and/or quantum chemistry have done) the quantity ω_e (as well as ω) the "vibrational frequency measured in cm^{-1}". The subscript "e" in ω_e stands for "equilibrium". The sense of this notation is the following: in the case of a harmonic oscillator, ω is a clearly defined quantity determined only by the values for the force constant and reduced mass; on the other hand, the quantity ω_e is just an empirical parameter appearing in experimentally derived formulae, such as Eq. (22). It would equal ω only if the correction terms (quadratic, cubic, *etc*.) in Eq. (22) were neglected. This is slightly misleading (see, *e.g*., recent papers in the present journal[6,7]), because the frequency, such as in the expressions $E = h\nu$ and $E = \hbar\omega$, has dimension s^{-1} (the former, ν, is the linear and the latter, ω, the angular frequency, $\omega = 2\pi\nu$). Herzberg's ω is actually the wave number, and formulae of the type (22) will be written in this paper as:

2012 Copyright (CC) SCS

$$E_{\mathrm{v}} \equiv T_{\mathrm{e}}hc + G(\mathrm{v})hc = \\ = T_{\mathrm{e}}hc + \left(\mathrm{v}+\frac{1}{2}\right)\tilde{\nu}hc - \left(\mathrm{v}+\frac{1}{2}\right)^2(\omega_{\mathrm{e}}x_{\mathrm{e}})hc + \left(\mathrm{v}+\frac{1}{2}\right)^3(\omega_{\mathrm{e}}y_{\mathrm{e}})hc + \ldots \quad (23)$$

where:

$$\tilde{\nu} \equiv \frac{1}{\lambda} = \frac{\nu}{c} = \frac{\omega}{2\pi c} \quad (24)$$

In Eq. (24), $\tilde{\nu}$ is the wave number (in cm^{-1}; to repeat, equal to Herzberg's ω_{e}), and λ it the wavelength, usually expressed in nm. However, the notations $\omega_{\mathrm{e}}x_{\mathrm{e}}$ and $\omega_{\mathrm{e}}y_{\mathrm{e}}$ will be retained for the experimentally determined anharmonicity parameters expressed in cm^{-1}, and the parentheses indicate that these formal products will be handled as single quantities. Note that the first cor-rection term in Eq. (22) appears with a minus sign. This choice was made because the energy distance between successive vibrational levels almost always decreases with increasing quantum number v, such that the quantity $\omega_{\mathrm{e}}x_{\mathrm{e}}$ is positive. On the other hand, the contribution of higher correction terms, such as $\omega_{\mathrm{e}}y_{\mathrm{e}}$, often negligible, can be either positive or negative.

3.3. Rotational structure of electronic transitions

If it is assumed that only the nuclei contribute to the moment of inertia of a diatomic molecule, that the molecule is in an $^1\Sigma^{\pm}$ electronic state and that it is a rigid rotator, then the rotation functions are spherical harmonics. In this case, the rotation energy levels are given by the formula:

$$E(J) = \frac{\hbar^2}{2I}J(J+1) = \frac{\hbar^2}{2\mu r_{\mathrm{e}}^2}J(J+1) \equiv BJ(J+1)hc \quad (25)$$

where

$$B \equiv \frac{\hbar^2}{2\mu r_{\mathrm{e}}^2 hc} = \frac{h}{8\pi^2 c\mu r_{\mathrm{e}}^2} \quad (26)$$

is the rotational constant, expressed in cm^{-1}, and the quantum number J takes the values 0, 1, 2,... Each energy level (except for $J = 0$ is $2J + 1$ degenerate, because the corresponding wave functions also depend on the value of the quantum number M, measuring the projection of the angular momentum on a space-fixed axis (Z). The projection of the angular momentum on the molecular axis equals zero. The selection rule for rotational transitions is $J' - J'' = 0, \pm 1$, with the restriction that the transition $J = 0 \leftrightarrow J = 0$ is forbidden.

However, the presence of electrons implies that the moment of inertia about the nuclear axis is not exactly zero, so that a diatomic molecule (if I_A is not

2012 Copyright (CC) SCS

neglected) should be handled as a prolate symmetric top rather than as a linear molecule. The energy formula (25) is then replaced by:

$$E(J) = \left[BJ\left(J+1\right) + \left(A-B\right)\Lambda^2 \right] hc \tag{27}$$

where $A \equiv \hbar^2/(2I_A hc) = h/(8\pi^2 c I_A)$, and Λ is the quantum number for the projection of the electronic angular momentum on the internuclear axis. For a given Λ, the quantum number J takes the values $J = \Lambda, \Lambda+1, \Lambda+2,\ldots$

The presence of the electron spin introduces coupling between electronic orbital, rotational and electronic spin degrees of freedom. There are several coupling schemes, known as the Hund's coupling cases.[4] The most widely applied are: case (a), covering the cases when the spin–orbit interaction is so strong that the projection, Σ, of the total electron spin on the molecule axis and consequently, the quantity $\Omega \equiv \Lambda + \Sigma$ is nearly conserved. In this case the "nearly good" quantum number Ω takes over the role of Λ from Eq. (27), *i.e.*, it represents the projection of J on the molecular axis and thus for a given Ω, the quantum number J takes the values $J = \Omega, \Omega+1,\ldots$; the other extreme represents a very weak spin–orbit coupling (Hund's case (b)). In this case, the electron spin is almost totally decoupled from the internuclear axis. The quantum numbers Σ and Ω are then not at all good, but instead N, representing the total angular momentum apart from spin, becomes a nearly good quantum number. Its projection on the internuclear axis is Λ.

The appearance of nearly good quantum numbers implies additional not strictly rigorous but useful (for classification of experimentally observed features) selection rules. In Hund's case (a), this is $\Delta\Sigma = 0$, and in case (b) $\Delta N = 0, \pm 1$ (again with the restriction that $\Delta N = 0$ does not occur in Σ–Σ electronic transitions). The only rigorous selection rule for rotational transitions is $\Delta J = 0, \pm 1$. However, even this rule ceases to be rigorous if the molecular nuclei have a non-vanishing spin. In such a case, the only rigorous selection rule is $\Delta F = 0, \pm 1$, where F is the quantum number for the total angular momentum involving also nuclear spins. However, because of the very weak coupling between the total angular momentum apart from nuclear spin and the nuclear spin, the selection rule $\Delta J = 0, \pm 1$ remains very strong.

Now, the simplest case of the rotational structure of an electronic transition is considered, namely, when both electronic states are of $^1\Sigma$ symmetry, and when the effects of anharmonicity can be neglected,. The selection rule for rotational transitions is then $J' = J'' + 1$ ("R branch") and $J' = J'' - 1$ ("P branch"). Let us take $J' = J$, then for the R branch, $J' = J'' + 1 = J + 1$, and the term values are:

$$\begin{aligned} \tilde{\nu} &= \tilde{\nu}_0 + F'\left(J'\right) - F''\left(J''\right) = \tilde{\nu}_0 + B'\left(J+1\right)\left(J+2\right) - B''J\left(J+1\right) = \\ &= \tilde{\nu}_0 + 2B' + \left(3B' - B''\right)J + \left(B' - B''\right)J^2 \end{aligned} \tag{28}$$

2012 Copyright (CC) SCS

where $\tilde{\nu}_0$ is a constant for the given electronic–vibrational transition, the "band origin". For the P branch, $J' = J'' - 1 = J - 1$, and the term values are thus:

$$\begin{aligned}\tilde{\nu} &= \tilde{\nu}_0 + F'(J') - F''(J'') = \tilde{\nu}_0 + B'(J-1)J - B''J(J+1) = \\ &= \tilde{\nu}_0 - (B'+B'')J + (B'-B'')J^2\end{aligned} \tag{29}$$

When $B' < B''$, the contribution of the quadratic term in J in Eq. (28) is negative, while the contribution of the linear term is positive (B' and B'' cannot differ very much from one another). At small J values, the linear term dominates but the difference in the contribution of the linear and quadratic terms becomes continuously smaller with increasing J; at a certain J value, $J = J_h$, they equalize, and after that the quadratic term becomes dominant. Around the $J = J_\mathrm{h}$ value (vertex of the parabola), the rotational lines are crowded and build a "band head". The band head appears at a wave number $\tilde{\nu}_\mathrm{h}$ higher than that of the band origin, *i.e.*, at the "violet side" with respect to $\tilde{\nu}_0$. The band is said to be "shaded" ("degraded") towards the red (*i.e.*, towards longer wave lengths). Conversely, when $B' > B''$ (this will be the situation for the case handled below), there is a band head in the P-branch on the red side with respect to the band origin, and this band is violet degraded. The position of the band head is found when the condition $\mathrm{d}\tilde{\nu}/\mathrm{d}J = 0$ is fulfilled. In the case when $B' > B''$, differentiating Eq. (29), one obtains:

$$J_\mathrm{h} = \frac{(B'+B'')}{2(B'-B'')} \tag{30}$$

Replacing in Eq. (29) J with J_h given by Eq. (30), one obtains for the term difference between the band head and the band origin (in the present case, there is no spectral line at the band origin, because the transition $J = 0 \leftrightarrow J = 0$ is forbidden):

$$\tilde{\nu}_\mathrm{h} - \tilde{\nu}_0 = -\frac{(B'+B'')^2}{4(B'-B'')} \tag{31}$$

In electronic transitions that do not involve two Σ species, in addition to the P and R branches, there is also a Q branch corresponding to the selection rule $\Delta J = 0$. The term values are:

$$\begin{aligned}\tilde{\nu} &= \tilde{\nu}_0 + F'(J') - F''(J'') = \\ &= \tilde{\nu}_0 + B'J(J+1) - B''J(J+1) = \tilde{\nu}_0 + (B'-B'')J(J+1)\end{aligned} \tag{32}$$

In electronic transitions between orbitally (Π, Δ, ...) and spin (doublet, triplet,...) degenerate species, there are several P, Q, and R sub-branches (sub-bands).

When the energies of rotational levels are determined by Eq. (25), each rotational level is $2J + 1$ degenerate. Since the rotational energy is in generally much smaller than the thermal energy, $\sim kT$, in usual spectroscopic experiments,

2012 Copyright (CC) SCS

the lowest-lying (J = 0) non-degenerate rotational level is, because of continuously increasing statistical weight with increasing J, less populated than some of the higher levels. Consequently, the maximum within a band consisting of rotational lines that correspond to the selection rule $J' - J'' = \pm 1$ is not at the "band origin" (the line that involves J' = 0 or J'' = 0) but instead at those J values for which an optimal compromise between two opposite tendencies, namely, an increase in the statistical weight and a decrease in the Boltzmann factor, $\exp\left|-E(J)/kT\right|$, is reached.

3.4. Spectral systems of MgO

When one starts with the (molecular) spectroscopic aspects of a problem, the first step is to look into two monographs. The first one is by Herzberg [4,9,10] – it actually consists of four volumes (the fourth one written in collaboration with Huber), plus a small additional book containing the heart of the first three monumental ones.[11] There is probably no other example in the scientific literature that the books written in the fifties of the preceding century that have lost almost nothing of their actuality. One only has to look at experimental papers published after that time and to complete in this way the information collected in Herzberg's books. Herzberg did it himself in the seventies and in his book (with Huber)[10] one can find all relevant data on diatomic molecules published until the end of 1975. Herzberg's (HH) books have become such a standard source of information on molecular spectra that many authors of new studies do not cite explicitly the authors of old experimental works but they simply quote them as "Herzberg and the references therein". This praxis will be followed in the present review. The other unavoidable book is that by Pearse and Gaydon (PG).[12] Its fourth (to our knowledge the last) edition was printed in 1976, *i.e.*, nearly at the same time as the Huber–Herzberg's compilation of data on diatomics. This edition contains the data published until the end of 1974. While the three volumes by HH also involve the complete theory underlying molecular spectra and numerical values for all possible molecular parameters, such as vibrational frequencies, anharmonicity and rotational constants, internuclear distances, *etc*. (this is reflected in the title of the series: "Molecular Spectra and Molecular Structure"), the book by PG (as the title, "The Identification of Molecular Spectra" says), only involves the results of direct spectral measurements, *i.e.*, the positions of band heads and their relative intensities. Thus, the books by HH and PG are in a sense complementary to each other: *e.g.*, in the HH books, one finds the transition energies in wave numbers, while they are collected by PG in wavelengths (this causes some difficulties when the results from these books are compared with one another; the numbers in HH's books correspond to vacuum and the band positions collected in PG to air, and thus the exact wavelength corresponding to a HH wave number cannot be obtained by simply inverting the last quantity). Those who still believe that it is possible to divide research into experi-

2012 Copyright (CC) SCS

mental and theoretical would say that the HH's books are aimed at theoreticians and that by PG at experimentalists.

Selected data for MgO, taken from HH,[10] are presented in Supplement B. HH constructed this table based on about 50 studies published from 1943 to 1975. All spectra observed until 1975 involved eight singlet and four triplet electronic states.

In the book by PG,[12] there are data about five spectral systems of MgO, namely of a strong green, a weaker red and three ultra-violet systems.

The red system appears in the wavelength range 690–470 nm and is assigned to the $B^1\Sigma^+$–$A^1\Pi$ electronic transition. The data in the PG monograph are taken from Mahanti and Lagerqvist and Uhler.[13–15] The spectrum was found to appear in the core of the magnesium arc in air, and in burning magnesium ribbon. Single-headed bands are degraded to the violet.

The information about the green system, assigned to the $B^1\Sigma^+$–$X^1\Sigma^+$ transition, was taken from Mahanti[13] and Lagerqvist.[16] This spectrum appears not only in a Mg arc in air, burning Mg ribbon, in flames, shock tubes and in the King furnace, but also in sun-spots. The spectral system is dominated by a very marked (0,0) sequence and the bands are degraded to the violet. The data for this system from the PG book are collected in Table I. The measured band position was used to calculate the vibrational term values in the $X^1\Sigma^+$ and $B^1\Sigma^+$ electronic states and to construct the corresponding Desladres table. In Table I, are also presented the term values computed by means of Eq. (23) using the vibrational frequencies and anharmonicity constants given in the literature.[10]

The information about violet systems of MgO, appearing between 396 and 364 nm, was based on several studies.[17–21] Two systems of red-degraded bands, $C^1\Sigma^-$–$A^1\Pi$ and $D^1\Sigma^-$–$A^1\Pi$, and a violet-degraded $^3\Delta$–$^3\Pi$ system were detected. In addition, Singh [22–24] reported on three other red-degraded ultra-violet systems appearing at 265.2 ($E^1\Sigma^+$–$X^1\Sigma^+$), 263.7 nm ($F^1\Pi$–$X^1\Sigma^+$) and 255.6 nm ($G^1\Pi$–$X^1\Sigma^+$). A violet-degraded band, assigned to $G^1\Pi$–$A^1\Pi$, was also detected at 275.01 nm.

Newer experimental studies, including optical spectroscopy, laser–magnet resonance, laser-induced fluorescence, two-colour resonance-enhanced two-photon ionization studies and vibrationally resolved photoelectron spectroscopy [25–37] have been cited in a recent theoretical study by Maatouk *et al.*[38]

Comparing the data collected by HH and PG, it could be stated that HH included in their book the $A^2\Sigma^+$–$X^2\Sigma$ systems in the (infra-red) region at about 1900 nm, which was only indirectly mentioned by PG. The reason might be that the first reference used by HH[39] appeared between the third and fourth editions of PG's book, and the second one[40] even later. Interestingly, neither HH nor PG cited the important study by Ghosh *et al.*[41] PG did not cite the paper by Lagerqvist and Uhler[42] and not even that by Pešić,[43] a former coworker of Gaydon. On

2012 Copyright (CC) SCS

the other hand, HH included in their book the results obtained by Antić-Jovanović *et al*. at the Faculty of Physical Chemistry in Belgrade.[44,45] Later, the results of the calculation of *FCF*s for the $B^1\Sigma^+$–$X^1\Sigma^+$ transition by Prasad and Prasad[46] will also be used.

TABLE I. Term values for bands of the green system, $B^2\Sigma^+$–$X^2\Sigma^+$ of MgO. The band heads (subscript h) are taken from ref. 12, and the band origins (subscript o) are computed by means of the formulae from ref. 10. The numbers without parentheses represent the original wavelengths in nm. Numbers in parentheses, without asterisks, in the central field of the table are the corresponding wave numbers (in cm^{-1}) obtained without an air–vacuum correction (*i.e.*, they are inverse values of the corresponding wavelengths). Based on them, the term values ($G_{v''}$, $T_{v'}$ and $G_{v'}$, subscript h) were calculated. The numbers in the central field given in parentheses with asterisks were obtained as differences of the derived term values

$T_{v'}$		$(19971)_h$	$(20753)_h$	$(21552)_h$	$(22320)_h$	$(23103)_h$	$(23877)_h$	–	–
$G_{v'}$		$(0)_h$	$(782)_h$	$(1581)_h$	$(2349)_h$	$(3132)_h$	$(3906)_h$	–	–
$T_{v'}$		20004_o	20818_o	21623_o	22418_o	23205_o	23981_o	24748_o	25506_o
$G_{v'}$		0_o	815_o	1620_o	2415_o	3201_o	3978_o	4745_o	5502_o
$G_{v''}$	v″	v′							
		0	1	2	3	4	5	6	7
$(0)_h$	0	500.73	481.85						
		(19971)	(20753)						
0_o		(19971)*	(20753)*						
		20004	20818						
$(762)_h$	1	520.60	499.67	481.01					
		(19209)	(20013)	(20790)					
775_o		(19209)*	(19991)*	(20790)*					
		19229	20043	20848					
$(1493)_h$	2		519.20	498.59	480.15				
			(19260)	(20057)	(20827)				
1539_o			(19260)*	(20059)*	(20827)*				
			19279	20084	20879				
$(2237)_h$	3			517.74	497.45				
				(19315)	(20103)				
2293_o				(19315)*	(20083)*				
				19330	20125				
$(2950)_h$	4				516.25	496.21			
					(19370)	(20153)			
3037_o					(19370)*	(20153)*			
					19381	20168			
$(3673)_h$	5					514.68	494.95		
						(19430)	(20204)		
3770_o						(19430)*	(20204)*		
						19435	20211		

2012 Copyright (CC) SCS

TABLE I. Continued

$G_{v''}$	v″	v′							
		0	1	2	3	4	5	6	7
4493_o	6							493.53 (20262) 20255	
5205_o	7								492.39 (20309) 20301

4. QUANTUM CHEMISTRY

At the beginning of nineties (of the previous century), the pope (actually, one of several) of quantum chemistry, W. Kutzelnigg, once said: "Twenty years ago, theoretical chemists claimed that they had calculated electronic transition energies with an uncertainty of 0.1 eV. They claim now that in these twenty years tremendous progress was achieved in their research field. However, if one asks them what the uncertainty in calculating electronic transition energies is today, they would say, 0.1 eV".

Working within the framework of his dissertation on several low-lying electronic states of HCN, the senior-coauthor of this review used in 1975 two atomic orbital (AO) basis sets. The smaller one consisted of 25 gaussians. It was found to be not flexible enough, and all the final calculations were performed with a "large" basis involving 27 AOs. The configuration-interaction (CI) space included roughly 20000 Slater determinants, about 2000 of them being selected for explicit calculations.[47] Ten years later, he tried to improve the results employing 50 gaussians, the CI space was chosen to consist of roughly 500000 determinants, and the secular problem actually solved was of dimensions up to 10000.[48] However, the new calculations did not bring anything substantially new. In favour of that speaks also the fact that the old study was cited (up to several years ago) 40 times, and the newer one only 16 times (indeed, it was accompanied by two additional papers, but the total number of citations for all three of them was comparable to that of the old paper). This tendency seems to continue. In the *ab initio* study discussed below, published in 2010,[38] solely the oxygen atom was described by 145 gaussians but the error margin remained at first sight the same as before. However, the reader should not come to the premature conclusion that nothing worthy has been realized in quantum chemistry since the seventies of the last century. First, in seventies, the usual error margin was 0.1–0.2 eV[49] and nowadays it is around 0.05 eV for the systems handled in this paragraph. That does not look spectacular, but recall that 0.2 eV corresponds to the difference between yellow and red (or yellow and green) colour, while 0.05 eV is only half a way between yellow and orange. Furthermore, molecules such as MgO and AlO do not belong to the easiest ones for *ab initio* computations.

2012 Copyright (CC) SCS

We do not insist that the title of this section is quite appropriate. It is only justified if one accepts the more historical than logical concept that molecules "belong" to chemistry, while atoms are a subject of physics. "Quantum chemistry" in its *ab initio* variant, commented above, is actually a kind of applied quantum mechanics. It would be more sensible to use the term quantum chemistry for investigations such a those carried out, *e.g.*, by Gutman *et al.*[50–59] However, in this case, a serious alternative to the name "quantum chemistry" would be "mathematical chemistry" or even something like "applied (mathematical) topology". This shows how difficult it is nowadays to classify scientific fields, particularly in terms of traditional categories.

4.1. MgO

The most extensive theoretical *ab initio* study on the MgO molecule was recently reported by Maatouk *et al.*[38] and the following discussion will rely on it. The preceding theoretical studies[30,60–72] performed on singlet and triplet electronic states will just be mentioned here. In them, equilibrium geometries, vibrational frequencies, excitation energies, transition moments and spin–orbit constants were determined for a number of electronic states lying up to 50000 cm^{-1} above the ground state. It was found that the ground state $X^1\Sigma^+$ represents an open-shell system because of the dominant Mg^+O^- form, and that the ionic–covalent interactions give rise to numerous avoided crossings between the potential energy curves.

Maatouk *et al.*[38] carried out the electronic structure calculations using the MOLPRO program suite.[73] The potential energy curves, electric TMs, and spin––orbit matrix elements were computed for a large number of singlet, doublet, and quintet electronic states by means of the complete active self-consistent field (CASSCF)[74] approach followed by the internally contracted multireference configuration interaction (MRCI) method,[75,76] with the cc-pV5Z AO basis sets.[77,78] Here, primarily, the results for the $X^1\Sigma^+$ and $B^1\Sigma^+$ electronic states (and the neighbouring species) will be considered, being involved in the transition that will be discussed below.

In the ground electronic state, $X^1\Sigma^+$, and not far from the equilibrium geometry (F–C region), the MgO molecule has two dominating electronic configurations, …$5\sigma^2$ $6\sigma^1$ $2\pi^4$ $7\sigma^1$ and …$5\sigma^2$ $6\sigma^2$ $2\pi^4$. At large Mg–O distances, the latter one predominates. In the F–C region, the lowest-lying excited electronic states of MgO are $a^3\Pi$ and $A^1\Pi$, both of them corresponding to the …$5\sigma^2$ $6\sigma^2$ $2\pi^3$ $7\sigma^1$ electronic configuration, and embedded only 0.2–0.4 eV above the ground state. The following two excited states are $b^3\Sigma^+$ and $B^1\Sigma^+$, the first of which has …$5\sigma^2$ $6\sigma^1$ $2\pi^4$ $7\sigma^1$ as the dominant configuration. The $B^1\Sigma^+$ state, with a vertical energy of about 2.5 eV ($T_e \approx 20000$ cm^{-1}), has in the F–C region, the same main electronic configurations as in the ground state. Consequently, the equilibrium bond lengths and vibrational frequencies are similar in the $B^1\Sigma^+$ and $X^1\Sigma^+$ states

2012 Copyright (CC) SCS

but these spectroscopic parameters are quite different from their counterparts in the other electronic species mentioned. Upon enlarging bond length, the $B^1\Sigma^+$ electronic state is continuously more dominated by the configurations …$5\sigma^2$ $6\sigma^2$ $2\pi^4$ and …$5\sigma^2$ $6\sigma^2$ $2\pi^2$ $6\sigma^2$, and thus at these geometries it differs considerably from the $X^1\Sigma^+$ state. Consequently, the electric TM between these two species shows a strong dependence on the bond length, as seen in Fig. 5 of Ref. 38. The other electronic states of MgO lie in the F–C region at considerably higher energies (> 3.5 eV).

The results of the *ab initio* study by Maatouk *et al.* are compared with the corresponding experimental findings in Table II. It is not our intension to analyse it; the only goal is to present the reader with the state of the art of modern *ab initio* computations. Just a small comment: look at the numbers 3558.50124 and 785.262621 cm^{-1} equivalent to the electronic transition energy and vibrational frequency, as given in the literature.[36] In our opinion, these are examples of senseless "accuracy" – even the natural width of spectral lines is much larger than the margin error quoted.

TABLE II. Comparison of *ab initio* results[38] with the corresponding experimental findings

State	T_e cm^{-1}	$(T_e)_{exp}$ cm^{-1}	$\tilde{\nu}$ cm^{-1}	$\tilde{\nu}_{exp}$ cm^{-1}	$\omega_e x_e$ cm^{-1}	$(\omega_e x_e)_{exp}$ cm^{-1}	r_e Å	$(r_e)_{exp}$ Å
$3^3\Delta$	52321		340.8		1.85		2.367	
$3^3\Sigma^-$	51748		337.5		2.03		2.356	
$2^1\Sigma^-$							∞	
$4^1\Pi$	44987.9		891.8		1.31		2.172	
$1^5\Pi$	41390.0		141.2		5.42		2.577	
$G^1\Pi$	40364.1	40259.8[a]	621.4		2.59		1.869	1.834[a]
$2^1\Delta$	39173.6		601.3		85.71		2.650	
$E^1\Sigma^+$	39113.1	37722[a]	698.1	705[a]	10.95	4.18[b]	1.837	1.829[a]
		37719[b]		714.2[b]				1.83[b]
$3^3\Pi$	38050.9	39967[l]	880.5		59.25		1.921	
$F^1\Pi$	37322.6	37922[a]	699.2	696[a]	5.12	4.5[c]	1.786	1.772[a]
		37919[c]		705[c]	6.9[d]			1.766[c]
				711[d]				1.77[d]
$2\ ^3\Sigma^-$	31520.3		798.4		28.95		1.991	
$e^3\Sigma^-$	30076	31250[a]					∞	∞[a]
$C^1\Sigma^-$	29516.1	30080.6[a]	626.9	632.4[a]	4.19	5.2[a]	1.886	1.873[a]
$D^1\Delta$	29228.2	29851.6[a]	625.1	632.5[a]	4.27	5.3[a]	1.886	1.8718[a]
		29835.4[e]		631.6[e]		5.2[e]		1.8606[e]
$d^3\Delta$	28930.5	29300[a]	653.5	650[a]	4.34	4.9[e]	1.875	1.87[a]
		29466.2[e]		655.2[e]				1.8710[e]
$2^3\Pi$	28218.4		283.4		1.61		2.799	
$c^3\Sigma^+$	27703.0	28300[a]	642.4		4.60		1.880	
$B^1\Sigma^+$	19332.7	19984.0[a,f,j]	808.2	824.08[a]	3.79	4.76[a]	1.753	1.737[a]
		19982.6[g]						
$b^3\Sigma^+$	7726.6		673.7		4.37		1.807	

2012 Copyright (CC) SCS

TABLE II. Continued

State	T_e cm^{-1}	$(T_e)_{exp}$ cm^{-1}	$\tilde{\nu}$ cm^{-1}	$\tilde{\nu}_{exp}$ cm^{-1}	$\omega_e x_e$ cm^{-1}	$(\omega_e x_e)_{exp}$ cm^{-1}	r_e Å	$(r_e)_{exp}$ Å
$A^1\Pi$	3078.5	3563.3[a,f]	654.3	664.4[a]	4.03	3.91[a]	1.879	1.864[a]
		3561.9[g]		664.3929[h]		3.9293[h]		1.864325[h]
		3563.8377[h]		664.3[i]		3.8[i]		1.8636[i]
		3560.1[i]		664.4765[j]		3.9264[j]		
		3563[j]		664.4360[k]		3.92853[k]		
		3558.50124[k]						
$a^3\Pi$	1645.4	2400[a]	644.8	650[a]	5.3		1.885	1.87[a]
		2492.5[l]		691.1[l]		4.0 [l]		1.8687[i]
		2623[g]		648[g]		3.9 [g]		
		2620.6[i]		648.3[m]		3.9 [m]		
		2618.9453[k]		650.2[i]		4.2 [i]		
				650.18028[k]		4.2 [k]		
$X^1\Sigma^+$	0	0	769.0	785.06[a,f]	4.45	5.18[a,f]	1.766	1.749[a]
		0		785.2183[j]		5.1327[j]		
		0		785.14[g]		5.07[g]		
		0		785.262621[k]		5.12379[k]		

[a]Ref. 10 and references therein; [b]ref. 35; [c]ref. 34; [d]ref. 37; [e]ref. 27; [f]ref. 42; [g]ref. 25; [h]ref. 29; [i]ref. 28; [j]ref. 32; [k]ref. 36; [l]ref. 33; [m]ref. 26

5. QUANTUM MECHANICS

5.1. Perturbative approach

The experimentally derived formulae (23) were either used directly or *via* Deslandres Tables constructed based on them for the assignment of the bands observed in our spectra (see, *e.g.*, Table I). However, for the determination of plasma temperatures, the FCFs and/or vibrational TMs are also required. In order to calculate these quantities, the vibrational Schrödinger Equation for the two electronic states in question has to be solved and the so-obtained wave functions used to compute the required quantities. In order to avoid explicit *ab initio* calculations of the potential curves for the electronic states in question, a way must first be found to extract the potential energy functions which, combined with the corresponding kinetic energy operator, give the energy eigenvalues as close as possible to those presented by formulae (23). This problem was solved by using quantum-mechanical perturbative and variational approaches.

The vibrational Hamiltonian in the form:

$$H = H^0 + V' \tag{33}$$

was assumed where:

$$H^0 = -\frac{\hbar^2}{2\mu}\frac{\mathrm{d}^2}{\mathrm{d}x^2} + \frac{1}{2}k^x x^2 \equiv \frac{1}{2}\left(-\frac{d^2}{d\xi^2} + \frac{1}{2}\xi^2\right)\hbar\omega \tag{34}$$

and

2012 Copyright (CC) SCS

$$V' = k_3^x x^3 + k_4^x x^4 \equiv \left(k_3 \xi^3 + k_4 \xi^4\right)\hbar\omega \tag{35}$$

where $x \equiv (r - r_e)$ is the difference between the instantaneous bond length, r, and its equilibrium value, r_e, and μ is the reduced mass. The dimensionless coordinate ξ, $\xi \equiv (\sqrt{\alpha})x$, where $\alpha \equiv (\mu\omega)/\hbar$, and $\omega = \sqrt{k/\mu}$ is the harmonic vibrational frequency (in s^{-1}), was introduced. k_3 and k_4 are the dimensionless cubic and quartic force constants, respectively, defined as:

$$k_3 \equiv \frac{1}{\alpha^{3/2}\hbar\omega} k_3^x \equiv \frac{\hbar^{1/2}}{\mu^{3/2}\omega^{5/2}} k_3^x, \quad k_4 \equiv \frac{1}{\alpha^2\hbar\omega} k_3^r \equiv \frac{\hbar}{\mu^2\omega^3} k_3^x \tag{36}$$

It is assumed that $|k_3| \gg |k_4|$, precisely that $|k_4|$ is at least by one order of magnitude smaller than $|k_3|$.

The eigenvalues of the zeroth-order, H^0, given by Eq. (34) are:

$$E_v^{(0)} = \left(v + \frac{1}{2}\right)\hbar\omega \tag{37}$$

and the corresponding wave functions are:

$$\psi_v^{(0)}(\xi) = N_v H_v(\xi) e^{-\frac{1}{2}\xi^2} \equiv |v\rangle \tag{38}$$

where N_v is the normalization factor and H_v is the Hermite polynomial. Applying the Rayleigh–Schrödinger perturbative approach (see, *e.g.*, ref. 79), the energy up to fourth order is obtained:

$$E_v = E_v^{(0)} + E_v^{(1)} + E_v^{(2)} + E_v^{(3)} + E_v^{(4)} \tag{39}$$

The corrections caused by the term $k_3^r r^3 \equiv k_3 \xi^3 \hbar\omega$ are (for details see Supplement C):

$$\begin{aligned} E_{v,3}^{(2)} &= -\frac{15}{4}\left(v + \frac{1}{2}\right)^2 k_3^2 \hbar\omega - \frac{7}{16} k_3^2 \hbar\omega \\ E_{v,3}^{(4)} &= -\frac{705}{16}\left(v + \frac{1}{2}\right)^3 k_3^4 \hbar\omega - \frac{1155}{64}\left(v + \frac{1}{2}\right) k_3^4 \hbar\omega \\ E_{v,3}^{(1)} &= E_{v,3}^{(3)} = 0 \end{aligned} \tag{40}$$

Since it is assumed that the energy contribution of the term $k_4^r r^4 \equiv k_4 \xi^4 \hbar\omega$ is much smaller than that of $k_3^r r^3 \equiv k_3 \xi^3 \hbar\omega$, it was found sensible to derive in this case only the results up to the second-order perturbation theory:

2012 Copyright (CC) SCS

$$E_{\mathrm{v},4}^{(1)} = \frac{3}{2}\left(\mathrm{v}+\frac{1}{2}\right)^2 k_4\hbar\omega + \frac{3}{8}k_4\hbar\omega$$
$$E_{\mathrm{v},4}^{(2)} = -\frac{17}{4}\left(\mathrm{v}+\frac{1}{2}\right)^3 k_4^2\hbar\omega - \frac{67}{16}\left(\mathrm{v}+\frac{1}{2}\right)k_4^2\hbar\omega \quad (41)$$

The next terms, $E_{\mathrm{v},3}^{(6)}, E_{\mathrm{v},4}^{(3)}$ would introduce the expressions proportional to $(\mathrm{v} + 1/2)^4$ and small corrections of the terms $(\mathrm{v} + 1/2)^p$ with $p \leq 3$, *etc*. (Actually, the one-dimensional oscillator is such a classical test-system in quantum mechanics that it is very probable that the formulae (40) and (41) have been derived many times before. However, we found it easier to rederive them than to find a source where they are presented). Thus, in the present approximation:

$$\begin{aligned}\frac{E}{\hbar\omega} &= \left(-\frac{7}{16}k + \frac{3}{8}k\right) + \left(\mathrm{v}+\frac{1}{2}\right)\left(1 - \frac{1155}{64}k - \frac{67}{16}k\right) + \\ &+ \left(\mathrm{v}+\frac{1}{2}\right)\left(-\frac{15}{4}k + \frac{3}{2}k\right) + \left(\mathrm{v}+\frac{1}{2}\right)\left(-\frac{705}{16}k - \frac{17}{4}k\right) \cong \\ &\cong \left(\mathrm{v}+\frac{1}{2}\right) - \left(\mathrm{v}+\frac{1}{2}\right)\left(\frac{15}{4}k - \frac{3}{2}k\right) + \left(\mathrm{v}+\frac{1}{2}\right)\left(-\frac{705}{16}k - \frac{17}{4}k\right)\end{aligned} \quad (42)$$

We can now establish the relation between the parameters determining the form of our vibrational Hamiltonian and the experimentally derived parameters $\tilde{\nu}$ (= Herzberg's ω_e), $\omega_\mathrm{e}x_\mathrm{e}$, $\omega_\mathrm{e}y_\mathrm{e}$, *etc*. The quadratic force constant from Eq. (34) is determined as:

$$k^x = \mu\omega^2 = 4\mu\pi^2c^2\tilde{\nu}^2 \quad (43)$$

To simplify the discussion, it is assumed now that the perturbation only contains the cubic term, and the perturbative energy formula is considered up to the second-order. The cubic force constants, k_3^x and/or k_3, are found by comparing the second term on the right-hand side of Eq. (23) with the second term on the right-hand side of Eq. (42) when $k_4 = 0$. It follows that:

$$k_3^x = \frac{2}{\sqrt{15}}\frac{\mu^{3/2}\omega^2}{\hbar}\sqrt{(\omega_\mathrm{e}x_\mathrm{e})hc} \quad (44)$$

It is convenient to replace the expressions (43) and (44) by the more practical working formulae:

$$\left[k_2(\mathrm{au})\right] = 3.7833\times10^{-8}\mu_r\left[\tilde{\nu}(\mathrm{cm}^{-1})\right]^2 \quad (45)$$
$$\left[k_3(\mathrm{au})\right] = 1.7810\times10^{-9}\mu_r^{3/2}\left[\tilde{\nu}\left(\mathrm{cm}^{-1}\right)\right]^2\left[\omega_\mathrm{e}x_\mathrm{e}\left(\mathrm{cm}^{-1}\right)\right]$$

2012 Copyright (CC) SCS

The force constants are now expressed in atomic units ($m_e \equiv 1$, $|e| \equiv 1$, $\hbar \equiv 1$), μ is assumed in relative atomic mass units ($\mu(^{12}C) \equiv 12$).

5.2. Variational approach

In variational calculations of eigenvalues and eigenfunctions of an anharmonic oscillator, as well as of the FCFs and TMs for particular combinations of vibrational levels of two electronic states, the following procedure is applied. One of the electronic states, *a* (typically the ground state), is chosen as the reference one and the basis functions (being the eigenfunctions of a suitably chosen harmonic oscillator) are centred with respect to its equilibrium bond length, r_e. If the potential energy curve is computed *ab initio*, it is fitted to the polynomial:

$$V_a = a_2 (r - r_e)^2 + a_3 (r - r_e)^3 + a_4 (r - r_e)^4 + \ldots \tag{47}$$

The Hamiltonian is then supposed in the form:

$$\begin{aligned} H_a = T + V_a = &-\frac{\hbar^2}{2\mu}\frac{d^2}{dr^2} + \frac{1}{2}k^r (r - r_e)^2 + \\ &+\left(a_2 - \frac{1}{2}k^r\right)(r - r_e)^2 + a_3 (r - r_e)^3 + a_4 (r - r_e)^4 + \ldots \end{aligned} \tag{48}$$

The eigenfunctions of the operator:

$$H^0 = -\frac{\hbar^2}{2\mu}\frac{d^2}{dr^2} + \frac{1}{2}k^r (r - r_e)^2 \tag{49}$$

are used as the basis.

Note that in Eq. (48), the quadratic part of the potential energy (47) is divided into two terms. The reason is that the eigenfunctions of a harmonic oscillator of the type (49) with a_2 instead of k^r could lead to a slower convergence of the results, particularly when the same basis functions for the description of other electronic states are employed (as will be done); if these states have equilibrium geometry significantly different from that of the reference state, it is to expect that more diffuse basis functions than the eigenfunctions of H^0 would be appropriate. Note also that the particular choice of k^r (except the mentioned one, namely, speed of convergence) has no other effect on the results of calculations. The potential energy curve of the other state, *b*, is fitted by polynomial series in the same variable as the reference state:

$$V_b = b_0 + b_1 (r - r_e) + b_2 (r - r_e)^2 + b_3 (r - r_e)^3 + b_4 (r - r_e)^4 + \ldots \tag{50}$$

where r_e is (as before) the equilibrium bond length in the ground electronic state. In this case, one also has a constant and a linear term in $(r - r_e)$, because the two states in question have different equilibrium bond lengths and their minima are separated in energy. The Hamiltonian for the *b* state is: $H_b = T + V_b$. Of course,

2012 Copyright (CC) SCS

instead of *ab initio* computed potentials, their experimentally derived counterparts could be used. As already stated, the corresponding Schrödinger equation is solved variationally. The variable $(r - r_e) \equiv x$ is replaced by its dimensionless counterpart, ξ, and the matrix elements are derived with the help of the formulae (C1–C4) from Supplement C (note that the matrix elements of the operator H^0, Eq. (49), are simply $H_{ij}^0 = (v+1/2)\hbar\omega\delta_{ij}$). To ensure convergent results for say 20 energy levels, not more than 30–40 basis functions are required. The eigenfunctions for the v″-th level of the electronic state *a* and the v′-th level of the state b are obtained in the form:

$$\left|\psi_{v''}\right\rangle = \sum_i c_i^{v''} \left|\psi_i^{(0)}\right\rangle, \; \left|\psi_{v'}\right\rangle = \sum_j d_j^{v'} \left|\psi_j^{(0)}\right\rangle \tag{51}$$

where $\left|\psi_i^{(0)}\right\rangle$ and $\left|\psi_j^{(0)}\right\rangle$ are the eigenfunctions of the operator (49), and $c_i^{v''}$ and $d_j^{v'}$ are the respective expansion coefficients. The advantage of the choice of the same basis for both states now becomes clear. The FCF for the two vibrational states in question is simply:

$$\left(FCF\right)_{v'v''} = \left[\sum_j d_j^{v'} \left\langle \psi_j^{(0)} \middle| \sum_i c_i^{v''} \middle| \psi_i^{(0)} \right\rangle\right]^2 = \left[\sum_i d_i^{v'} c_i^{v''}\right]^2 \tag{52}$$

When the bond-length dependence of the electric TM is taken into account, it is fitted to the form:

$$R^{e',e''} = \sum_k R'_k \left(r - r_e\right)^k \equiv \sum_k R'_k \, x^k \equiv \sum_k R'_k \, \alpha^{-\frac{k}{2}} \xi^k \equiv \sum_k R_k \xi^k \tag{53}$$

($R_k \equiv \alpha^{-k/2} R'_k$) and the vibrational TM is computed as:

$$\begin{aligned} R^{e'v',e''v''} &= \sum_j d_j^{v'} \left\langle \psi_j^{(0)} \middle| \sum_k R_k \xi^k \sum_i c_i^{v''} \middle| \psi_i^{(0)} \right\rangle = \\ &= \sum_i \sum_j \sum_k d_j^{v'} R_k c_i^{v''} \left\langle \psi_j^{(0)} \middle| \xi^k \middle| \psi_i^{(0)} \right\rangle \end{aligned} \tag{54}$$

A general disadvantage of the presented variational approach is that it is not able to describe properly the vibrational states lying close to the dissociation limit; at $x \to \infty$, each polynomial tends to $+\infty$ or to $-\infty$, while the potential curve for a real bound state, asymptotically tends to a horizontal line. However, in the present study, only low-lying vibrational levels are considered and this drawback of the method does not play any role.

2012 Copyright (CC) SCS

6. DETERMINATION OF PLASMA COMPOSITION

In one of the next sections, the results of the calculation of the equilibrium composition of plasmas containing Mg, O and H are presented. These calculations were performed by means of a self-written computer program following the approach developed by White *et. al.*[80] This method is described in Supplement D – in this section, only the key points are presented.

For the determination of the equilibrium composition of a gas mixture, the only quantity needed is the molal standard (Gibbs) free energy function G^0. The Gibbs energy of a mixture of n chemical species containing x_i moles of the i-th species can be expressed as:

$$G(X) = \sum_{i=1}^{n} x_i f_i \tag{55}$$

$X = \{x_1, x_2, ..., x_n\}$ $X = \{x_1, x_2, \ldots, x_n\}$ is a set of mol numbers, and f_i is the chemical potential of the i-th species, given by:

$$f_i = G_i^0 + RT \ln p_i = G_i^0 + RT \ln\left(\frac{x_i}{\bar{x}} P\right) \equiv \left(c_i + \ln \frac{x_i}{\bar{x}}\right) \tag{56}$$

In Eq. (56), the notation:

$$c_i = G_i^0 + RT \ln p \tag{57}$$

$$\bar{x} = \sum_{j=1}^{n} x_i \tag{58}$$

is introduced, where T is the temperature and p is the total pressure of the system. Thus, Eq. (55) can be rewritten in the form:

$$G(X) = \sum_{i=1}^{n} x_i \left(c_i + \ln \frac{x_i}{\bar{x}}\right) \tag{59}$$

Let it be supposed that one starts with a mixture of atoms of m elements and that the number of atoms of the element j is proportional to b_j. The determination of the equilibrium composition is equivalent to finding the set of non-negative values of x_i which minimize (59) and satisfy two conditions: *i*) the mass balance constraint:

$$\sum_{i=1}^{n} x_i a_{ij} = b_j, \quad (j = 1, 2, ..., m) \tag{60}$$

where a_{ij} is the number of atoms of element j in the chemical species (atom, molecule or ion) i and *ii*) the charge balance condition,[81]

2012 Copyright (CC) SCS

$$\sum_{i=1}^{n} x_i a_i = 0 \tag{61}$$

where a_i is the charge number of species i. The summation in Eq. (61) formally runs over all chemical species, but this sum actually only involves the contributions from atomic and molecular ions and electrons. It is convenient to write Eqs. (60) and (61) as a single system:

$$\sum_{i=1}^{n} x_i a_{ij} = b_j, \quad (j = 1,\ 2,\ ...,\ m+1) \tag{62}$$

where $b_{m+1} = 0$ and $a_{i,m+1} = a_i$. Starting with any positive set of values $X^{(0)} = \{x_1^{(0)}, x_2^{(0)}, \ldots, x_n^{(0)}\}$ that satisfies the conditions (62), and form the expression analogous to (59), one obtains the optimal coefficients $X = \{x_1, x_2, \ldots, x_n\}$ that lead to the condition $\partial G(X) / \partial x_i = 0$ for all x_i, by applying the iterative approach described in Supplement D.

This algorithm has been used in numerous calculations of plasma composition.[81–96] The free energy data are taken from JANAF Thermochemical Tables,[97] or computed using derived partition functions based on previous quantum chemical calculations of molecular structure parameters.[6,7,98–100]

7. PLASMA ELECTROLYTIC OXIDATION

Plasma electrolytic oxidation (PEO) is high-voltage anodizing process employed to produce relatively thick oxide coatings on valve metals, such as magnesium, aluminium and titanium, with the incorporation of species originating both from the substrate and electrolyte. During anodization, two types of oxide films can grow, barrier and porous oxide ones.[101] The type of an oxide film is primarily determined by the type of electrolyte and by the anodizing conditions. The thickness of compact barrier oxide films is limited to several hundreds nm due to the dielectric breakdown initiated during film growth. Anodization of metals above the breakdown voltage is followed by an intense generation of sparks.[102] Thick and hard oxide coatings formed by the anodic-spark deposition method can range from tens to hundreds of microns. They consist of a thin barrier layer adjacent to the metal, followed by an intermediate layer with relatively low porosity, and an outer layer containing large pores, cracks and channels. Porous oxide films are formed in electrolytes that partially dissolve oxide films.[103] Such films consist of two regions: an outer one of thick porous-type oxide and a thin compact inner region lying adjacent to the metal. The thickness of the porous oxide films can grow to hundreds of microns.

Anodization of metals is accompanied by the emission of a weak electromagnetic radiation, mostly in the visible region of the spectrum.[104–109] This process is termed galvanoluminescence (GL) or electroluminescence.[110] GL has

2012 Copyright (CC) SCS

been investigated by many authors but explanations of the nature and the mechanism of GL are still not completely resolved, because of the complex environment and the many experimental parameters that determine the intensity and spectral distribution of GL. During the past several years, a group from the Faculty of Physics of the University of Belgrade have conducted a number of investigations of the GL during the anodization of aluminium and showed that the nature and GL intensity depend on the type of the electrolyte (organic or inorganic), surface pre-treatment and anodizing conditions.[111–118]

There are two main reasons for investigating GL: The first one is that it (combined with other kinds of measurements) yields information about the system considered, particularly about the microstructure of the oxide films formed in the anodization process. The second reason is that the discharge built during this process is a convenient medium for the occurrence of a number of spectral lines and bands and thus, it can serve as a source of new spectroscopic information.

Surface pre-treatment of samples (surface preparation and annealing) has a significant influence on GL obtained in inorganic electrolytes. In fact, the pre-treatment of samples governs the concentration of "flaws" in oxide films, which are related to the GL mechanism.[111–113,116] "Flaws" is a general term for micro-fissures, cracks, local regions of different compositions and impurities, *etc*. The annealing temperature of the samples is another pre-treatment factor that affects the GL intensity. Higher annealing temperatures result in higher GL intensities. Annealing at different temperatures has various influences on the state of the surface of a sample, the number of defects, crystal grains and their orientation, in other words, on the concentration of "flaws". The GL of oxide films formed by anodization of aluminium samples annealed at temperatures above 500 °C showed that the sudden rise in the formation of gamma crystalline regions caused by aluminium annealing is strongly related to the appearance of GL and its intensity.[114,115,118] An analysis based on literature data on simple molecular species involving the Al atom, as well as those atoms whose presence was possible under given experimental conditions (hydrogen, oxygen, *etc*.), showed that the sources of GL are the molecules AlH, AlO, Al_2 and AlH_2, related to the formation of islands of gamma alumina crystals at annealing temperatures above 500 °C. In the case of organic electrolytes, GL is agitated by collision of electrons, injected into the oxide film at the electrolyte–oxide interface and accelerated by the high electric field (nearly 10^7 V cm^{-1}), with luminescence centres (carboxylate ions) inside the oxide film.[106,107]

Anodization of metals above the breakdown voltage leads to formation of a plasma, as indicated by the presence of microdischarges on the metal surface, accompanied by gas evolution.[109,110] Various processes, including chemical, electrochemical, thermodynamical and plasma-chemical reactions, occur at the discharge sites, due to the increased local temperature (10^3 to 10^4 K) and pres-

2012 Copyright (CC) SCS

sure (up to ~10^2 MPa) that modify the structure, composition and morphology of oxide coatings.

Given the liquid environment, optical emission spectroscopy (OES) is the best available technique for PEO plasma characterization. The main difficulty in the application of OES for PEO characterization comes from space and time inhomogeneity of the microdischarges appearing randomly across the anode surface. The first step in the application of OES for PEO is the identification of the atomic and ionic lines in the visible and near UV spectral region.[120–130] Relative line intensity measurements of species originating in the substrate or in the electrolyte were used for the determination of the electron temperature.[121,123,124,126,128,132] The spectral line shape analysis of hydrogen Balmer lines were used for an estimation of the electron density.[122,123,126–128] The molecular vibrational temperature was determined from the luminescence of AlO[129] and MgO.[131]

8. EXPERIMENTAL

In the experiment to be described,[131] samples of a magnesium alloy (96 % Mg, 3 % Al, and 1% Zn (Goodfellow) with dimensions 25 mm×5 mm×0.25 mm were used as the working electrodes. They were sealed with insulation resin leaving only an active surface with an area of 1.5 cm^2. Before the anodization, the samples were degreased in acetone, ethanol and distilled water, using an ultrasonic cleaner, and dried in a warm-air stream. The magnesium alloy was anodized in an aqueous solution containing 4 g L^{-1} $Na_2SiO_3 \cdot 5H_2O$ and 4 g L^{-1} KOH. The electrolyte was prepared using double distilled and deionised water and *p.a.* grade chemical compounds. During anodization, the current density was set to 150 mA cm^{-2}.

A schematic diagram of the experimental setup used for the luminescence measurements is shown in Fig. 1. The anodization occurred in an electrolytic cell with flat glass windows.[107] Two platinum wires (5 cm long, 1 mm in diameter) were used as cathodes. The power supply was a self-made DC power unit providing voltages of 0–600 V and a current of 0–500 mA. During the anodization, the electrolyte was circulated through the chamber-reservoir system, and a control temperature sensor was situated immediately by the sample. The temperature of the electrolyte was kept fixed at 20±1 °C.

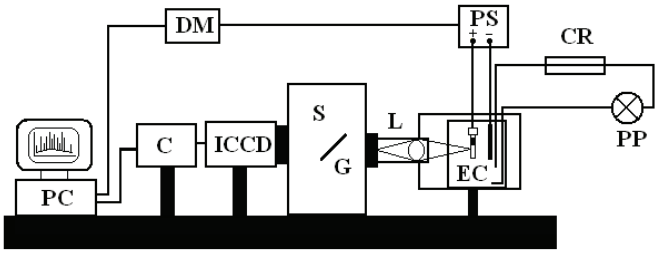

Fig. 1. Schematic diagram of the experimental setup used for the luminescence measurements: EC – electrolytic cell; PS – power supply; PP – peristatical pump; CR – chamber-reservoir system; L – achromatic lens; S – spectrograph Hilger; G – diffraction grating (1200 grooves mm^{-1}); ICCD – intensified charge coupled device; C – controller ST-133; DM – digital multimeter HP 34970A; PC – personal computer.

2012 Copyright (CC) SCS

The spectral luminescence was taken on a spectrometer system based on an intensified charge coupled device (ICCD). The optical detection system consisted of a large-aperture achromatic lens, a Hilger spectrometer with diffraction grating of 1200 grooves mm^{-1} (wavelength range of 43 nm), and a very sensitive PI–MAX ICCD thermoelectrically cooled camera (–40 °C) with a high quantum efficiency (Princeton Instruments). The system was used with several grating positions with an overlapping wavelength range of 5 nm. The image of anode surface was projected with unity magnification to the entrance slit of the spectrometer. The optical detection system was calibrated using a light emitting diodes based light source.[133] The spectra were adjusted to the spectral response of the measuring system. The anodization voltage and the electrolyte temperature were recorded by a 20-channel digital PC-controlled multimeter HP 34970A (DM).

9. RESULTS AND DISCUSSION

9.1. Luminescence of the $B^1\Sigma^+$–$X^1\Sigma^+$ system of MgO during PEO of Mg

In recent years, several research groups were focused on the investigation of PEO as a surface-protective treatment for magnesium and its alloys.[134–138] Despite numerous studies on metals, primarily on Al, in which OES was used for the characterization of PEO, there are only few such papers on Mg.[128,130,131,139,140] Herein, the results of our recent study on this species are presented.[131]

In the initial phase of anodization of the magnesium alloy, the voltage increased linearly with time to about 220 V, resulting in a constant rate of increase of the oxide film thickness. Simultaneously, a weak anodic luminescence was observed. This stage of anodization was followed by a deflection from linearity in the voltage curve, starting from the so-called breakdown voltage. During this phase of the process, a large number of sparks appeared, randomly distributed over the surface. Sparking luminescence combined with the anodic one and the total luminescence intensity increased. After the breakdown, the oxide surface became laced with a number of cracks, pores and channels (Fig. 2).

A number of emission spectral atomic and ionic lines were recorded in the wavelength range from 370 to 850 nm (*i.e.*, from 11800 to 27000 cm^{-1}). The species that were identified[141] (K, Na, Mg, H_α and O) originated from both the magnesium electrode and the electrolyte. We refrained from using these lines for the determination of plasma parameters, such as temperature and electron density: The spectral resolution was relatively low, so that some of the lines were overlapped, the strong alkali metal lines were at least partly self-absorbed and finally, the sensitivity of the measurements depended on the wavelength, making comparison of lines appearing in different spectral regions difficult.

9.2. $B^1\Sigma^+$–$X^1\Sigma^+$ *Spectrum of MgO*

Now, focus was directed on the wave number range between 19950 and 20400 cm^{-1}. A number of spectra at different time delays with respect to the beginning of the PEO process were recorded. A typical spectrum is presented in

2012 Copyright (CC) SCS

Fig. 3. It appears as a broad peak with clearly pronounced structure. The most intense sub-peak is at 19976 cm^{-1}, and the other sub-peaks are blue-shifted with respect to it. While the overall intensity of the broad peak presented in Fig. 3 significantly varied with time, the relative intensities of the sub-peaks within it showed quite small variations. The below used results for relative intensity of the local peaks were obtained by averaging over about 30 recorded spectra. The positions of the sub-peaks are presented in column Exp. 5 of Table III. They were assigned, as will be shown below, to the $v' - v'' = 0$ band sequence of the $B^1\Sigma^+ - X^1\Sigma^+$ emission transition of MgO.

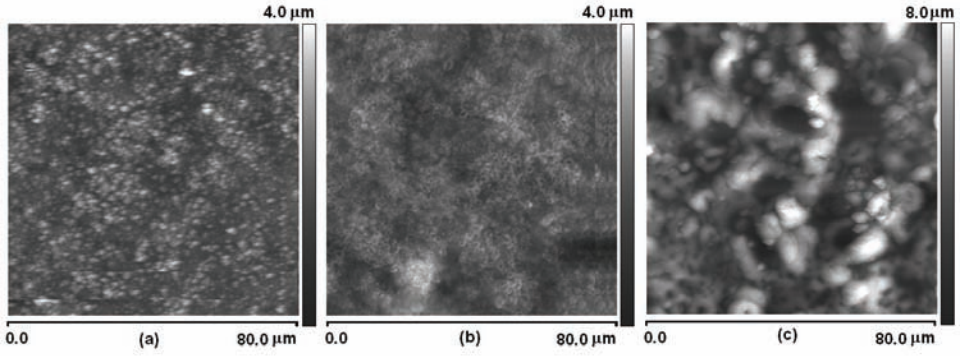

Fig. 2. Atomic force microscopy image of the oxide coating on the magnesium alloy formed after breakdown (anodization time 5 min).[131]

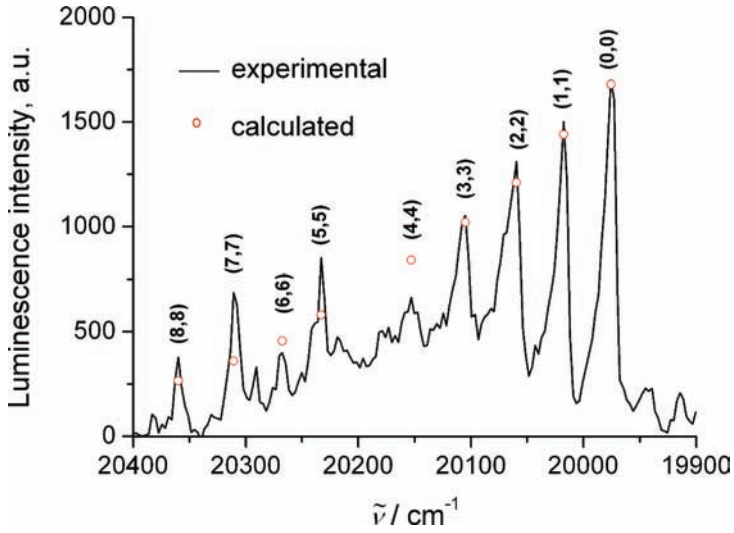

Fig. 3. Luminescence spectrum between 19950 and 20400 cm^{-1} obtained after subtracting the anodic luminescence contribution.[131] The peaks are assigned to (v', v'') bands of the $B^1\Sigma^+ - X^1\Sigma^+$ system of MgO. The circles denote the intensities of the peaks as obtained in the simulation procedure described in the text.

2012 Copyright (CC) SCS

TABLE III. Positions (in cm^{-1}) of the v′ – v″ = 0 band heads ($\tilde{\nu}_h$) and origins ($\tilde{\nu}_0$) of the $B^1\Sigma^+$–$X^1\Sigma^+$ spectral system of MgO. In parentheses are given the term values relative to the position of the 0–0 band[131]

Para-meter	Exp. 1[41] $\tilde{\nu}_h$	Exp. 2[16] $\tilde{\nu}_h$	Exp. 3[43] $\tilde{\nu}_h$	Exp. 4[12] $\tilde{\nu}_h$	Exp. 5[131] $\tilde{\nu}_h$	Fit 1[41] $\tilde{\nu}_h$	Fit 2[43] $\tilde{\nu}_h$	Fit 3[43] $\tilde{\nu}_0$	Fit 4[10] $\tilde{\nu}_0$	Fit 5[131] $\tilde{\nu}_0$
T_e						19950		19983.97	19984.0	
$\tilde{\nu}'$						754		796.08	824.08	
$(\omega_e,x_e)'$						3.06		4.44	4.76	
$\tilde{\nu}''$						722		758.38	785.06	
$(\omega_e,x_e)''$						5.96		4.84	5.18	
0–0	19966 (0)	19965 (0)	19967 (0)	19971 (0)	19976 (0)	19967 (0)	19966 (0)	20003 (0)	20004 (0)	20004 (0)
1–1	20007 (41)	20007 (42)	20008 (41)	20013 (42)	20018 (42)	20005 (38)	20008 (41)	20041 (38)	20044 (40)	20044 (40)
2–2	20049 (83)	20051 (86)	20049 (82)	20057 (86)	20060 (84)	20049 (82)	20049 (83)	20081 (78)	20084 (81)	20084 (81)
3–3	20093 (127)	20097 (132)	20092 (125)	20103 (132)	20106 (130)	20098 (131)	20092 (125)	20121 (118)	20126 (122)	20127 (123)
4–4	20146 (180)		20137 (170)	20153 (182)	20153 (177)	20153 (186)	20134 (168)	20162 (159)	20168 (164)	20171 (167)
5–5	20200 (234)			20204 (233)	20231 (255)	20215 (248)		20203 (200)	20211 (208)	20216 (213)
6–6	20257 (291)			20262 (291)	20268 (292)	20281 (314)		20245 (243)	20255 (252)	20265 (261)
7–7	20304 (338)			20309 (338)	20310 (334)	20354 (387)		20289 (286)	20300 (297)	20316 (312)
8–8	20347 (381)				20360 (384)	20433 (466)		20333 (330)	20346 (342)	20372 (368)
9–9	20388 (422)					20517 (550)		20377 (374)	20393 (389)	20434 (430)

A brief analysis of previous experimental studies on the *B*–*X* spectral system of MgO is here presented. In several studies, the rotational constants for the $X^1\Sigma^+$ and $B^1\Sigma^+$ states were precisely determined (Table II). It was found that they are very similar in both electronic states, with that for the upper state being slightly larger. The similarity of the equilibrium bond lengths and vibrational frequencies, as well as the fact that the *B*–*X* system involves the $^1\Sigma$ species, determines the general structure of the spectrum. It is dominated by the v′ – v″ = 0 band sequence and the bands have *P* and *R* branches. The position of the P band heads ($\tilde{\nu}_h$) with respect to the band origins ($\tilde{\nu}_0$) can be estimated by means of the Formula (31) with B'' = 0.5743 cm^{-1} and B' = 0.5822 cm^{-1};[10] one obtains $\tilde{\nu}_h - \tilde{\nu}_0 \cong 40\ cm^{-1}$. This large difference reflects the similarity of the rotational constants for the $X^1\Sigma^+$ and $B^1\Sigma^+$ states. The positions of the band heads and band origins for the v′ – v″ = 0 sequence, as measured or fitted by various authors, are given in Table III.

2012 Copyright (CC) SCS

The vibrational structure of the blue–green band system was investigated by Ghosh *et al*.[41] The authors recorded about thirty violet-degraded emission bands in the wave number region between 19000 and 21000 cm^{-1} and assigned them to the sequences $v' - v'' = 0, \pm 1$, with the vibrational quantum number *v* up to ten. In the second column of Table III (Exp. 1), the experimental results for the heads of the $v' - v'' = 0$ bands are presented. In all previous studies, the positions of the $B^1\Sigma^+$–$X^1\Sigma^+$ bands were fitted by various formulas of the type Eq. (23), quadratic in the vibrational quantum numbers. The parameters $T_e, \tilde{\nu}$ and $\omega_e x_e$ given by Ghosh *et al*. as well as the term values computed using them are presented in the seventh column of Table III (Fit 1). Comparison of the numbers in columns Exp. 1 and Fit 1 shows that only the position of the bands up to 4–4 are reliably reproduced by Formula (23).

The same band system was later investigated by Mahanti,[13] Lagerqvist and Uhler[16,42] and Pešić.[19,43] The experimental results of Lagerqvist[16] and Pešić [43] are shown in columns Exp. 2 and Exp. 3, respectively. The band positions adopted by PG,[12] taken from the studies of Mahanti[13] and Lagerqvist,[16] are presented in column Exp. 4. Pešić[43] adopted from Lagerquist and Uhler[42] the parameters $T_e, \tilde{\nu}$, and $\omega_e x_e$ for the positions of the band origins, corrected them to take into account the difference between the positions of the band origins and band heads and obtained by means of Formula (3) the term values collected in column Fit 2. They agreed well with his own experimental results from column Exp. 3. However, when the original parameters by Lagerquist and Uhler (given at the top of column Fit 3) were used to calculate the origins of the bands with $v' = v'' \geq 5$, as shown in column Fit 3, the agreement with the corresponding experimental data from columns Exp. 1 and Exp. 4 (the numbers in parentheses) becomes poor.

The most reliable parameters for the values of the vibrational term are those presented in the HH book,[10] column Fit 4, because they (in contrast to those used by Ghosh *et al*. and Pešić) involved the correct vibrational frequencies. However, even they do not describe accurately the positions of $v' = v'' \geq 4$ bands. Thus, no hitherto applied formula quadratic in the vibrational quantum number v has given good reproduction of the measured band positions for higher v values. This is easy to explain: The differences in the wave numbers of the successive bands observed (column Exp. 4) are 42, 44, 46, 50, 51, 58 and 47 cm^{-1}, and they nearly follow quadratic dependence only for first few terms. This will be born in mind in the following discussion.

Bearing in mind the restrictions caused by specific features of our experiment, the results of the study,[131] column Exp. 5 of Table IV, were found to agree reasonably with previous more precise gas-phase spectral measurements. Namely, the accuracy of the measured band heads was estimated to be roughly ±5 cm^{-1}. Furthermore, the position of the bands depended to a certain extent on the matrix conditions, and it was not possible to resolve the features corresponding to

2012 Copyright (CC) SCS

isotopic species ^{24}MgO, ^{25}MgO, and ^{26}MgO, the last two each present in relative fractions of about 0.10.

TABLE IV. Franck–Condon factors (first row for each quantum number v″), and squared vibrational moments (third row) for transitions between vibrational levels of the $X^2\Sigma^+$ and $B^2\Sigma^+$ electronic states of MgO (our study[131]). Second row: results of previous studies

v″	v′						
	0	1	2	3	4	5	6
0	.9826	.0170	.0004				
	.983[a]	.017[a]	.000[a]				
	1.421	.0089	.0003[b]				
			.0002				
1	.0173	.9464	.0351	.0011			
	.017[a]	.948[a]	.033[a]	.001[a]			
	.0480	1.344	.0375[b]	.0001			
			.0180				
2		.0364	.9067	.0544	.0024		
		.035[a]	.911 [a] .901 [b]	.053 [a] .0576 [b]	.0018 [b]		
		.0969			.0011		
			1.263	.0274			
3		.0002	.0573	.8632	.0751	.0042	
		.000[a]	.053[a]	.881[a]	.0804[b]	.0033[b]	
		.0017	.0606[b]	.857[b]	.0371	.0019	
			.1471	1.179			
4			.0005	.0801	.8154	.0972	.0067
			.0010[b]	.061[a]	.806[b]	.105[b]	.0029
			.0039	.0827[b]	1.090	.0472	
				.1981			
5				.0011	.1049	.7626	.1212
				.0075	.108[b]	.752[b]	.0577
					.2494	.9963	
6					.0022	.1317	.7041
					.0035[b]	.135[b]	.8974
					.0130	.3005	

[a]Ref. 46; [b]ref. 25

9.3. Computation of F–C factors and vibrational transition moments

FCFs and vibrational TMs for the $B^1\Sigma^+$–$X^1\Sigma^+$ system of MgO were calculated by means of the approaches described in Section 5, "Quantum mechanics". The potential energy part of the Hamiltonian was assumed in the form of polynomials of the third order in the coordinate $x \equiv (r - r_e)$. In this paragraph, the potential energy and the bond length are expressed in atomic units; thus the energy is given in hartree (1 hartree = 27.211 eV) and the bond length in bohr (1 bohr = 0.529177 Å). The force constants k_2 and k_3 were determined by means of

2012 Copyright (CC) SCS

Formulae (45) and (46), employing the molecular parameters from Ref. 10 (*i.e.*, those appearing in the table presented in Supplement B), giving:

$$V\left(X\ ^1\Sigma^+\right) = 0.111991x^2 - 0.07426x^3,$$
$$V\left(B\ ^1\Sigma^+\right) = 0.0910532 + 0.12331\left(x + 0.0225\right)^2 - 0.07844\left(x + 0.0225\right)^3 \quad (63)$$

where $\Delta r_e = -0.0225$ bohr is the difference between the equilibrium bond lengths in the excited and ground electronic state. Thus, both potentials in Eq. (63) are given with respect to the equilibrium bond lengths in the ground state. The form of the electric moment for the transition between the $B^1\Sigma^+$ and $X^1\Sigma^+$ states was estimated based on Fig. 4 of the *ab initio* study:[38]

$$R_{e',e''}\left(\text{au}\right) = -1.2 + 0.7x \quad (64)$$

The Schrödinger equation (63) with the potentials was solved variationally, as described above.

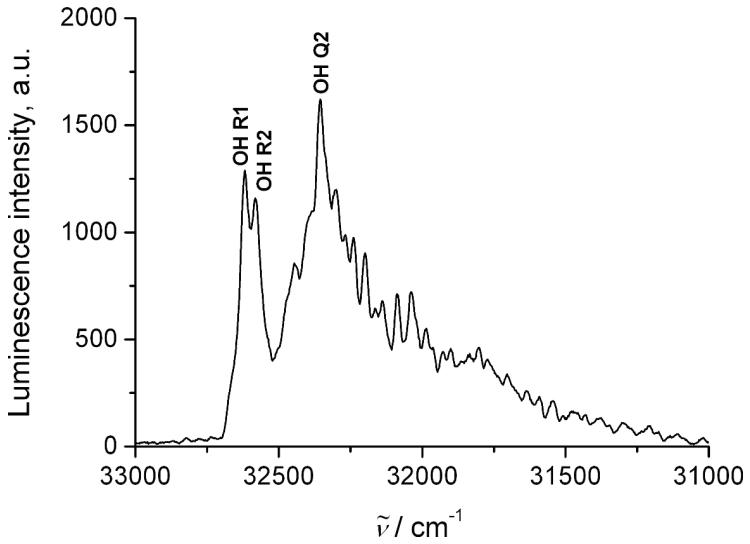

Fig. 4. $A^2\Sigma^+$ (v′ = 0)–$X^2\Pi$ (v″ = 0) luminescence spectrum of OH between 31000 and 33000 cm^{-1}.[131]

The results for the band origins are presented in the last column of Table IV (Fit 5). For low vibrational quantum numbers (up to v′ = v″ = 3), they coincide with the numbers in the column Fit. 4, generated by employing Formulae (23) with the same set of molecular parameters. The agreement becomes continuously poorer with increasing v′ = v″ ≥ 4, reflecting the restricted reliability of the second-order perturbative approach used to determine the force constants which appear in the Formulae (63). The computed FCFs and squared vibrational TMs for

2012 Copyright (CC) SCS

levels up to v = 6 are given in Table IV. The FCFs computed by Prasad and Prasad[46] and those quoted by Ikeda *et al.*[25] are given in column F–C_{exp}. The agreement between these three sets of results, particularly for larger FCFs, is very good. This indirectly indicates that also the computed vibrational TMs are reliable. The ratio (TM^2/FCF) decreases uniformly with increasing vibrational quantum number within the v′ – v″ = 0 sequence, reflecting the decrease of the absolute value of the electric TM with increasing bond length (see Fig. 5a).

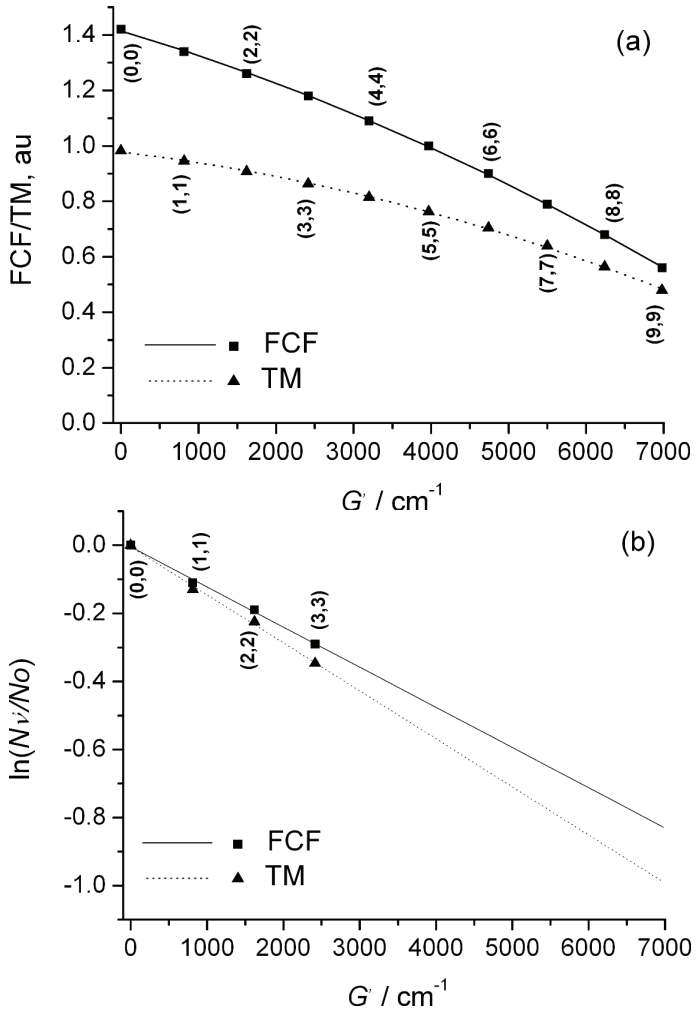

Fig. 5. a) Calculated Franck–Condon factors (*FCF*) and squared vibrational transition moments (TM) for the v′ = v″ band sequence of the $B^1\Sigma^+$–$X^1\Sigma^+$ system of MgO, as functions of vibrational quantum number, *i.e.*, of the vibrational term values of the $B^1\Sigma^+$ electronic state; b) logarithm of the relative population of the v′ = 0, 1, 2, and 3 vibrational levels as function of the corresponding term values.[131]

2012 Copyright (CC) SCS

9.4. Estimation of the population of vibrational levels and determination of plasma temperature

The relative population, $N_{v'}$, of the vibrational levels in the $B^1\Sigma^+$ electronic state was estimated by means of the procedure described in Section 3, "Spectroscopy". It was obtained for the levels v′ from 0 to 3 as the ratio of the measured intensity of the peaks corresponding to the (0–0), (1–1), (2–2), and (3–3) transitions and the corresponding (squared) vibrational TMs. The values for ln ($N_{v'}/N_{v'=0}$) as function of the vibrational term values (G')/quantum numbers of the $B^1\Sigma^+$ electronic state are displayed in Fig. 4b. The nearly linear dependence of ln ($N_{v'}/N_{v'=0}$) on the G' leads to the conclusion quasi-equilibrium conditions existed, at least for vibrational motions. The slope of the straight line, $-1/kT$, determines the plasma temperature of $T \approx 11500$ K. When the TMs are replaced by the corresponding FCFs, $T \approx 9800$ K is obtained. The difference between these two temperature values shows that it is important to account for the variation of the electronic transition moment with the bond length. Taking into account the limited accuracy of the present experimental results (the accuracy of measured intensities was roughly estimated to be 10 %), as well as of the *ab initio* computed electric transition-moment function, it was considered justified to conclude that the temperature of the plasma was $T = 11000\pm2000$ K. This value is not very different from that obtained in a study on AlO ($T = 8000\pm2000$ K).[129] Assuming $T = 11000$ K and using the vibrational TMs for v′ = v″ = 0–8, the complete v′ – – v″ = 0 band sequence of the $B^1\Sigma^+$–$X^1\Sigma^+$ system of MgO is simulated in Fig. 3. In spite of some discrepancies between the experimental and simulated results, the general agreement could be considered satisfactory.

9.5. Estimation of the plasma temperature based on the use of OH bands

We additionally determined the plasma temperature by means of the $A^2\Sigma^+$–$X^2\Pi$ (v′ = v″ = 0) emission spectrum of OH, employing the approach of de Izarra.[142] Four groups of unresolved rotational lines were recorded with the maxima at 32364, 32484, 32597 and 32622 cm^{-1}, corresponding to the Q_2, Q_1, R_2, and R_1 band heads, respectively (Fig. 5). Using Tables 2–5 from Ref. 142, the temperature was estimated to be 3500±500 K.

9.6. Calculation of the plasma composition

At first sight the difference between the temperature estimated by means of the intensity distribution within the MgO band system and that derived from the unresolved rotational spectrum of OH should be a clear indication for the absence of a local thermal equilibrium (LTE) in the plasma. In the first case, one is namely dealing with the vibrational and in the second case, with the rotational temperature, and the possibility that these two motion modes are not in equilibrium with each other must be taken into account. However, there are also other pos-

2012 Copyright (CC) SCS

sible explanations. Let it be noted that temperatures similar to those of the present study were reported by several authors.[121,122,143,144] Based on experimental results, Klapkiv[143,144] proposed a model of the discharge plasma consisting of a central core (containing electrons, ionic and atomic species) with the temperature at roughly 7000 K, surrounded by lower-temperature regions involving various compounds formed in chemical reactions between the species originating both in the substrate and the electrolyte. Arrabal *et al.*[139] and Hussein *at al.*[128,140] estimated a plasma temperature of 7000 K. Dunleavy *et al.*[122] determined the temperature of the peripheral zone to be about 3500 K by comparing the intensities of the H_α and H_β Balmer lines, while the use of Mg^+ and Si^+ lines yielded T = 16000±3500 K for the plasma core temperature. Employing these data, as well as those for the electron density, they concluded that the LTE conditions were fulfilled in the plasma core, while the colder peripheral region was found to be in partial LTE.

Now, the consequences of the assumption of the LTE for all degrees of freedom under the present experimental conditions will be investigated. Employing the method described in Section 6, the composition of a plasma containing Mg, O and H, at temperatures up to T = 12000 K and for pressures of 10^5, 10^6, 10^7 and 10^8 Pa, was calculated. Pressures in such a wide region were considered because it was argued that in systems similar to the present one they might be up to ≈10^2 MPa.[145] Since the amounts of Mg, O and H in the investigated plasma were unknown, the computations were performed at Mg:O:H ratios of 1:1:1, 1:1:0, 0:1:1, and 0:1:2 in order to estimate the influence of a particular choice on the conclusions which could be reached on the basis of the results. The free energy data for 26 atomic/ionic/molecular species involving Mg, O and H (plus electrons) collected in JANAF tables[97] were extended by an extrapolation procedure from 6000 to 12000 K. Some of the results are presented in Figs. 6 and 7.

The results for a pressure of 10^5 Pa (*i.e.*, nearly 1 atm) and at Mg:O:H = = 1:1:1 are presented in Fig. 6. At T = 11000 K, 90 % of magnesium is in form of Mg^+ and 10 % appears as Mg, while the partial pressure of MgO is about $1/10^5$ of the total pressure. Slightly below T = 9000 K, the partial pressures of Mg and Mg^+ become equal, and at lower temperatures atomic Mg is the dominating form of magnesium. The most abundant form of magnesium in the temperature region below T = 3000 K is MgOH. The concentration of OH reaches a maximum in the temperature region between 3000 and 4000 K. Increasing the total pressure favours the building (*i.e.*, suppresses dissociation) of MgO, and suppresses the ionization process $Mg \rightarrow Mg^+ + e^-$. Consequently, at a total pressure of 10^6 Pa (Fig. 6b of ref. 131), the partial pressures of Mg and Mg^+ are nearly equal at 11000 K, and roughly 0.1 % of the magnesium is in form of MgO. At $p = 10^7$ Pa (Fig 6c in ref. 131) and T = 11000 K, about 2 % of the magnesium is in form of MgO. Finally, at $p = 10^8$ Pa (Fig. 7) and T = 11000 K, the partial pressure of MgO ex-

2012 Copyright (CC) SCS

ceeds that of Mg^+, becoming only four times lower than that of the most abundant magnesium species, atomic Mg.

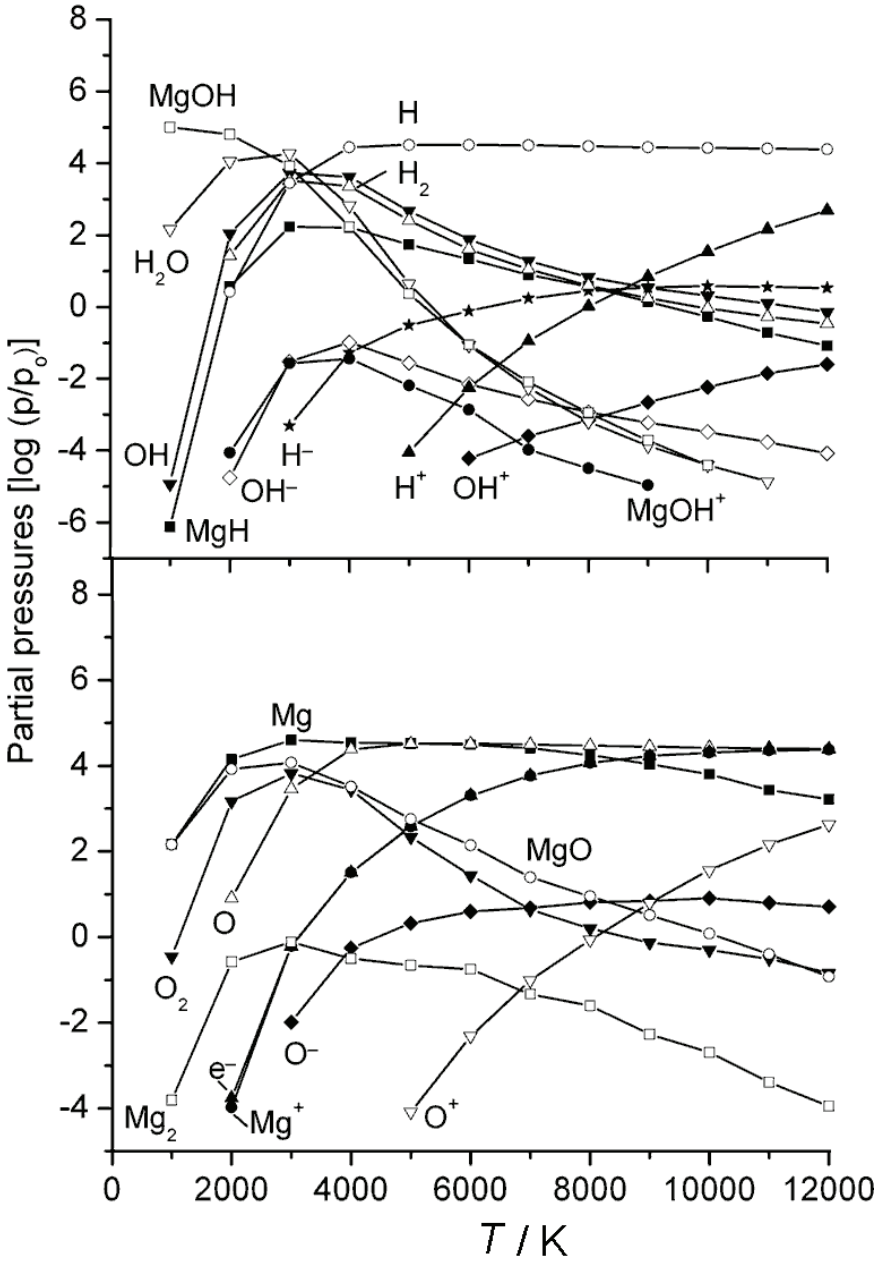

Fig. 6. Equilibrium composition of the plasma containing a mixture of magnesium, oxygen, and hydrogen in the mole ratio 1:1:1 at $p = 10^5$ Pa.[131]

2012 Copyright (CC) SCS

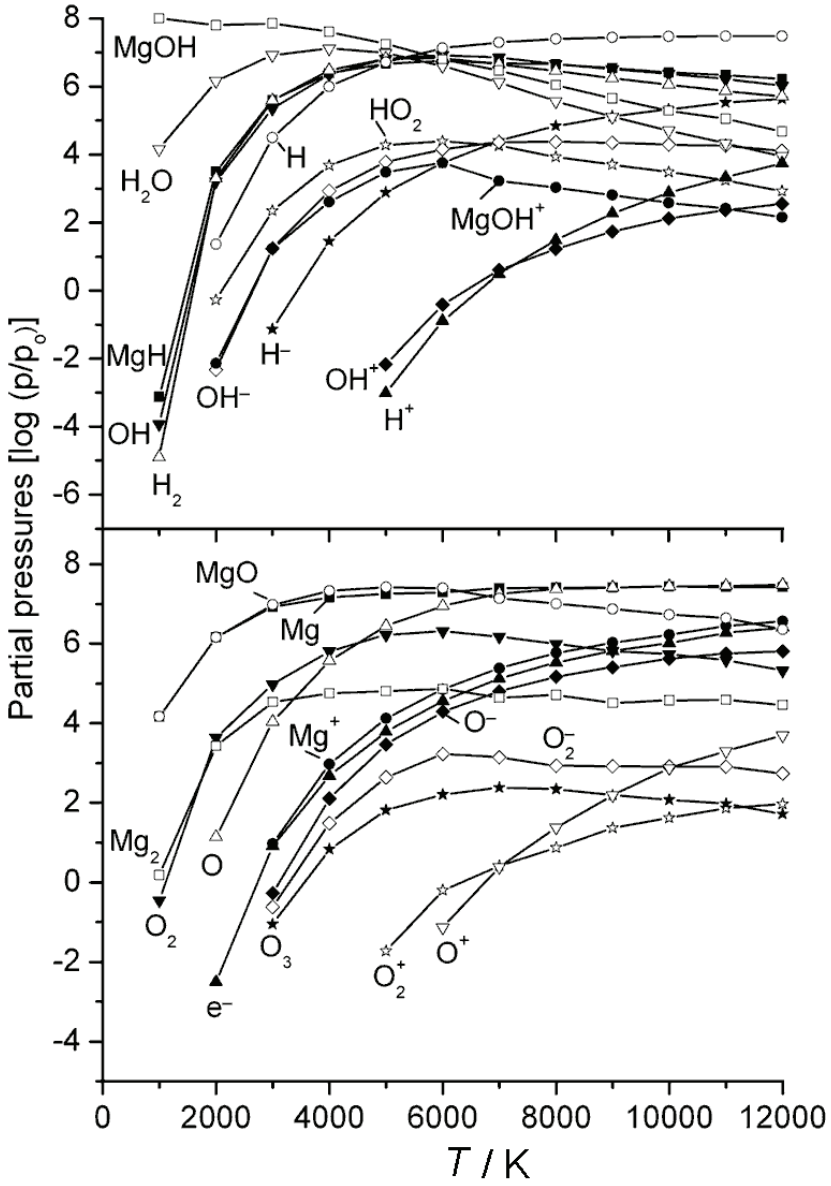

Fig. 7. Equilibrium composition of plasma containing a mixture of magnesium, oxygen, and hydrogen in the mole ratio 1:1:1 at $p = 10^8$ Pa.[131]

Now an attempt will be made to interpret our experimental results in the light of the calculated plasma compositions.[131] The first question concerns the reliability of the value of T = 11000 K, based on the intensity distribution within the $B^1\Sigma^+$–$X^1\Sigma^+$ band system of MgO. Is it possible to obtain this molecular spec-

2012 Copyright (CC) SCS

trum at such a high temperature? First, it should be noted that in LTE, the population of the $B^1\Sigma^+$ electronic state of MgO would be about 7 % with respect to that of the ground state at T = 11000 K. Thus, it would be large enough to cause the appearance of an emission spectrum if the MgO molecules were present in a sufficient concentration at this temperature. The results of the above calculations of the plasma composition show that this is the case when the pressure in the plasma core is higher than the normal one. This is illustrated in Fig. 8, in which the temperature dependence of the function $p_{MgO}\times\exp(-E/kT)$ is shown, where $E \approx 20000\ \mathrm{cm}^{-1}\times hc$, being the excitation energy for the $B^1\Sigma^+$ electronic state, and p_{MgO} is the partial pressure of MgO at different pressures. Two sets of results are presented; the first (full lines) correspond to a plasma with the global composition Mg:O:H = 1:1:1, and the second one (dotted lines) to a plasma without hydrogen, *i.e.*, with the global composition Mg:O:H = 1:1:0. Note that the distributions $p_{MgO}\times\exp(-E/kT) = f(T)$ are practically same in both cases (except for a systematic shift of the dotted lines towards larger values) at each particular pressure. This shows that the relative amounts of Mg, O and H, assumed in calculations do not critically influence the general conclusions that could be drawn.

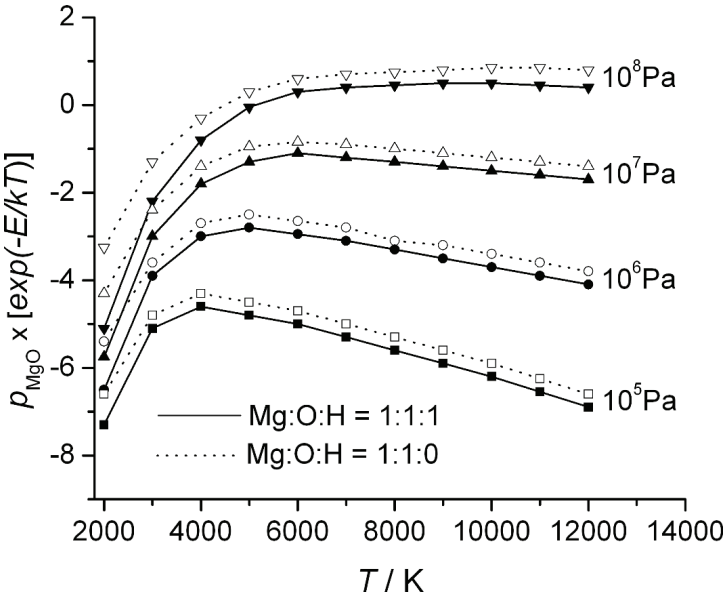

Fig. 8. Temperature dependence of $p_{MgO}\times\exp(-E/kT)$, where E is the excitation energy for the $B^1\Sigma^+$ electronic state, at various pressures for the global plasma composition Mg:O:H = 1:1:1 (full lines) and Mg:O:H = 1:1:0 (dotted lines).[131]

How reliable is the lower temperature value ($T \approx 3500$ K), based on the measured OH spectrum? Let the problem be sharpened: suppose that it is certain that an LTE exists and that the approaches for estimating the temperature T = 3500 K

2012 Copyright (CC) SCS

from the OH band and T = 11000 K from the MgO bands are completely exact. Does this necessarily mean that there are only these two temperatures characterizing the plasma? Is it not possible that there is a relatively large region of the plasma where the temperature is, say, 5000 K, but the OH and MgO spectra are not obtained from this region because the temperature is too high for existence of OH molecules and too low for excitation of the MgO molecules? In order to answer this question, the function $p_{OH}\times\exp(-E/kT) = f(T)$ is shown in Fig. 9 (at the moment, we concentrate solely on OH; an analogous analysis could be applied to MgO), where $E \approx 32600$ cm$^{-1}\times hc$ is the excitation energy for the $A^2\Sigma^+$ electronic state and p_{OH} is the partial pressure of OH. Due to near cancellation of the effect of decrease in p_{OH} and increase in $\exp(-E/kT)$ with increasing T, there is almost no dependence of $p_{OH}\times\exp(-E/kT)$ on T in the temperature region between 4000 and 12000 K, independently of the pressure and global plasma compositions considered. The intensity of the OH bands should be even higher if the temperature in the region where the OH molecules exist were higher than the estimated T = 3500 K. Two conclusions can be drawn: the OH molecules are formed and exist only in the peripheral, colder plasma region; the temperature gradient between the peripheral region and the plasma core is very high, having as a consequence a very narrow plasma region with intermediate temperatures. The second conclusion supports the Klapkiv model,[143,144] and is in accordance with the results by

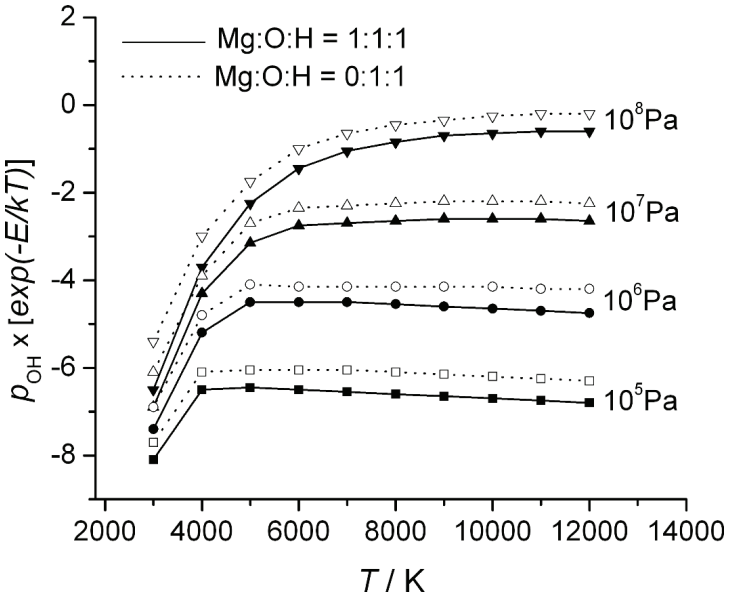

Fig. 9. Temperature dependence of $p_{OH}\times\exp(-E/kT)$, where E is the excitation energy for the $A^2\Sigma^+$ electronic state of OH, at various pressures for the global plasma composition Mg:O:H = 1:1:1 (full lines) and Mg:O:H = 0:1:1 (dotted lines).[131]

2012 Copyright (CC) SCS

Dunleavy *et al.*[122] who obtained, using a completely different method, a low-region temperature identical to that of the present study.

10. CONCLUSIONS

The research described in the present review began in the field of material science. The starting goal was to investigate the behaviour of metal alloys in the process of plasma electrolytic oxidation. Special electronics, optics, microscopy and crystallography were needed to enquire the morphology of the material, particularly of the thin oxide films produced. In order to obtain information about the processes which occurred, with the aim to become able to monitor them, luminescence spectra were recorded. Their identification led into the field of atomic and molecular spectroscopy. The understanding, and in certain cases even assignment of molecular features recorded, would not have been possible without the use of results of quantum-chemical calculations. On the other hand, it turned out that the systems in question could serve as a source of new spectroscopic information. For an estimation of important parameters, such as temperature and electron number density, various plasma diagnostics methods had to be applied. The results of measurements of molecular spectra were combined with quantum-mechanical calculations for an estimation of the plasma parameters when the standard approaches failed. In order to understand the appearance of the spectra, and the features of the system they originate from, the compositions of the plasmas in question were calculated. This required the use of methods of classical and statistical thermodynamics. The message of the present review is just to show how many different scientific fields encompass an, at first glance, simple research problem.

SUPPLEMENTARY MATERIAL

Supplements A–D are available electronically from http://www.shd.org.rs/JSCS/, or from the corresponding author on request.

Acknowledgements. We thank the Ministry of Education, Science and Technological Development of the Republic of Serbia for financial support (Contract No. 172040).

И З В О Д

ЈЕДНА МУЛТИДИСЦИПЛИНАРНА СТУДИЈА НА МАГНЕЗИЈУМУ

РАДОМИР РАНКОВИЋ[1], СТЕВАН СТОЈАДИНОВИЋ[2], МИРЈАНА САРВАН[2], БЕЋКО КАСАЛИЦА[2], МАРИЈА КРМАР[1], ЈЕЛЕНА РАДИЋ-ПЕРИЋ[1] и МИЉЕНКО ПЕРИЋ[1]

[1]Факултет за физичку хемију Универзитета у Београду и [2]Физички факултет Универзитета у Београду

У току плазмене електролитичке оксидације једне легуре магнезијума (96% Mg, 3% Al и 1% Zn) добили смо галванолуминисцентни спектар у области таласних бројева између 19950 и 20400 cm^{-1}. Широки пик са јасно израженом структуром приписан је v − v = 0 секвенцији електронског прелаза $B^1\Sigma^+ \rightarrow X^1\Sigma^+$ молекула MgO. Применом квантномеханичке теорије пертурбације, из положаја спектралних трака изведена је

2012 Copyright (CC) SCS

форма кривих потенцијане енергије за оба електронска стања. Ове потенцијалске криве, комбиноване са квантнохемијски израчунатим електричним моментом прелаза, коришћене су у варијационом рачунању Франк–Кондонових фактора и момената прелаза за опажене вибрационе прелазе. Поређењем резултата ових рачуна са измереном расподелом интензитета у спектру извели смо релативну запоседнутост вибрационих нивоа горњег електронског стања. То је омогућило процену температуре плазме. Температура је додатно одређена на основу снимљеног емисионог спектра $A^2\Sigma^+$ (v = 0)–$X^2\Pi$ (v = 0) радикала OH. Под претпоставком постојања локалне термодинамичке равнотеже израчунат је састав плазме која садржи магнезијум, кисеоник и водоник, у области темепратуре до 12000 K за притиске од 10^5, 10^6, 10^7, and 10^8 Pa, да би се објаснила појава регистрованог спектра и допринело расветљавању процеса који се догађају за време електролитичке оксидације Mg.

(Примљено 12. септембра, ревидирано 10. октобра 2012)

REFERENCES

1. W. F. McDonough, *The Composition of the Earth*, in *Earthquake Thermodynamics and Phase Transformations in the Earth's Interior*, R. Teisseyre, E. Majewski, Eds., Academic Press, San Diego, CA, 2001
2. J. W. Morgan, E. Anders, *Proc. Nat. Acad. Sci. U.S.A.* **77** (1980) 6973
3. A. P. Dickin, *In situ Cosmogenic Isotopes, Radiogenic Isotope Geology*, Cambridge University Press, Cambridge, UK, 2005
4. G. Herzberg, *Molecular Spectra and Molecular Structure I. Spectra of Diatomic Molecules*, Van Nostrand, New York, 1955
5. M. Perić, in *Electron – A Hundred Years from Discovery*, Sveska prva, Milan Kurepa, Ed., Zavod za udžbenike i nastavna sredstva, Belgrade, 1997, p. 311 (in Serbian)
6. M. Senćanski, J. Radić-Perić, M. Perić, *J. Serb. Chem. Soc.* **76** (2011) 539
7. M. Senćanski, Lj. Stojanović, S. Jerosimić, J. Radić-Perić, M. Perić, *J. Serb. Chem. Soc.* **76** (2011) 557
8. G. Herzberg, *Molecular Spectra and Molecular Structure II. Infrared and Raman Spectra of Polyatomic Molecules*, Van Nostrand, New York, 1945
9. G. Herzberg, *Molecular Spectra and Molecular Structure III. Electronic Spectra of Polyatomic Molecules*, Van Nostrand, New York, 1967
10. K. P. Huber, G. Herzberg, *Molecular Spectra and Molecular Structure IV. Constants of Diatomic Molecules*, Van Nostrand, New York, 1979
11. G. Herzberg, *The Spectra and Structure of Simple Free Radicals*, Cornel University Press, Ithaca and London, 1971
12. R. W. B. Pearse, A. G. Gaydon, *The Identification of Molecular Spectra*, Chapman and Hall, London, 1976
13. P. C. Mahanty, *Phys. Rev.* **42** (1932) 609
14. P. C. Mahanty, *Indian J. Phys.* **9** (1935) 455
15. A. Lagerqvist, U. Uhler, *Nature* **164** (1949) 665
16. A. Lagerqvist, *Ark. Mat. Astron. Fys.* **A29**, No. 25 (1943) 1
17. L. Brewer, R. F. Porter, *J. Chem. Phys.* **22** (1954) 1867
18. D. Pešić, A. G. Gaydon, *Proc. Phys. Soc.* **73** (1959) 244
19. D. Pešić, *Proc. Phys. Soc.* **76** (1960) 844
20. L. Brewer, S. Trajmar , R. A. Berg, *Astrophys. J.* **135** (1962) 955
21. S. Trajmar, G. E. Ewing, *Astrophys. J.* **142** (1965) 77

2012 Copyright (CC) SCS

22. M. Singh, *J. Phys., B* **4** (1971) 565
23. M. Singh, *J. Phys., B* **6** (1973) 1339
24. M. Singh, *J. Phys., B* **6** (1973) 1917
25. T. Ikeda, N. B. Wong, D. O. Harris, R. W. Field, *J. Mol. Spectrosc*. **68** (1977) 452
26. B. Bourguignon, J.C. McCombie, J. Rostas, *Chem. Phys. Lett*. **113** (1985) 323
27. B. Bourguignon, J. Rostas, *J. Mol. Spectrosc*. **146** (1991) 437
28. P. C. F. Ip, K. J. Cross, R. W. Field, J. Rostas, B. Bourguignon, J. McCombie, *J. Mol. Spectrosc*. **146** (1991) 409
29. E. Kagi, T. Hirano, S. Takano, K. Kawaguchi, *J. Mol. Spectrosc*. **168** (1994) 109
30. P. Mürtz, H. Thümmel, C. Pfelzer, W. Urban, *Mol. Phys*. **86** (1995) 513
31. J. H. Kim, X. Li, L. S. Wang, H. L. de Clercq, C. A. Fancher, O. C. Thomas, K. H. Bowen, *J. Phys. Chem., A* **105** (2001) 5709
32. J. W. Daily, C. Dreyer, A. Abbud-Madrid, M. C. Branch, *J. Mol. Spectrosc*. **214** (2002) 111
33. D. Bellert, K. L. Burns, N.-T. Van-Oanh, J. Wang, W. H. Breckenridge, *Chem. Phys. Lett*. **381** (2003) 381
34. D. Bellert, K. L. Burns, N.-T. Van-Oanh, J. Wang, W. H. Breckenridge, *Chem. Phys. Lett*. **381** (2003) 725
35. J. Wang, N.-T. Van-Oanh, D. Bellert, W. H. Breckenridge, M.-A. Gaveau, E. Gloaguen, B. Soep, J.-M. Mestdagh, *Chem. Phys. Lett*. **392** (2004) 62
36. E. Kagi, K. Kawaguchi, *J. Mol. Struct*. **795** (2006) 179
37. J. Wang, W. H. Breckenridge, *J. Chem. Phys*. **124** (2006) 124308
38. A. Maatouk, A. Ben Houria, O. Yazidi, N. Jaidane, M. Hochlaf, *J. Chem. Phys*. **133** (2010) 144302
39. L.-B. Knight, Jr., W. Weltner, Jr., *J. Chem. Phys*. **55** (1971) 5066
40. S. Rosenwaks, R. E. Steele, H. P. Broida, *J. Chem. Phys*. **63** (1975) 1963
41. P. N. Ghosh, P. C. Mahanty, B. C. Mukkerjee, *Phys. Rev*. **35** (1930) 1491
42. A. Lagerqvist, U. Uhler, *Ark. Fys*. **1** (1949) 459
43. D. S. Pešić, *Proc. Phys. Soc*. **83** (1964) 885
44. A. Antić-Jovanović, D. S. Pešić, V. Bojović, *J. Mol. Spectrosc*. **60** (1976) 416
45. A. Antić-Jovanović, V. Bojović, D. S. Pešić, *J. Phys., B* **9** (1976) L575
46. S. S. Prasad, K. Prasad, *Proc. Phys. Soc*. **80** (1962) 311
47. M. Perić, S. D. Peyerimhoff, R. J. Buenker, *Can. J. Chem*. **20** (1077) 3664
48. M. Perić, H. Dohmann, S. D. Peyerimhoff, R. J. Buenker, *Z. Phys. D* **5** (1987) 65
49. M. Perić, *Bull. Soc. Chim. Beograd* **44** (1979) 465
50. S. Radenković, I. Gutman, *J. Serb. Chem. Soc.* **74** (2009) 155
51. J. Đurđević, I. Gutman, R. Ponec, *J. Serb. Chem. Soc.* **74** (2009) 549
52. I. Gutman, J. Đurđević, *J. Serb. Chem. Soc.* **74** (2009) 765
53. B. Furtula, I. Gutman, S. Jeremić, S. Radenković, *J. Serb. Chem. Soc.* **75** (2010) 83
54. S. Jeremić, S. Radenković, I. Gutman, *J. Serb. Chem. Soc.* **75** (2010) 943
55. D. Vukičević, J. Đurđević, I. Gutman, *J. Serb. Chem. Soc.* **75** (2010) 1093
56. S. Marković, J. Đurđević, S. Jeremić, I. Gutman, *J. Serb. Chem. Soc.* **75** (2010) 1241
57. I. Gutman, B. Furtula, A. T. Balaban, *J. Serb. Chem.* **76** (2011) 733
58. I. Gutman, A. T. Balaban, *J. Serb. Chem. Soc.* **76** (2011) 1505
59. M. Marković, J. Đurđević, I. Gutman, *J. Serb. Chem. Soc.* **77** (2012) 751
60. J. Schamps, H. Lefebvre-Brion, *J. Chem. Phys*. **56** (1972) 573
61. S. R. Langhoff, C. W. Bauschlicher, Jr., H. Partridge, *J. Chem. Phys*. **84** (1986) 4474

2012 Copyright (CC) SCS

62. H. Thümmel, R. Klotz, S. D. Peyerimhoff, *Chem. Phys*. **129** (1989) 417
63. A. F. Jalbout, *J. Mol. Struct*. **618** (2002) 85
64. C. W. Bauschlicher, Jr., D. M. Silver, D. R. Yarkony, *J. Chem. Phys*. **73** (1980) 2867
65. C. W. Bauschlicher, Jr., B. H. Lengsfield III, M. Silver, D. R. Yarkony, *J. Chem. Phys*. **74** (1981) 2379
66. C. W. Bauschlicher, Jr., S. R. Langhoff, H. Partridge, *J. Chem. Phys*. **101** (1994) 2644
67. C. W. Bauschlicher, H. Partridge, *Chem. Phys. Lett*. **342** (2001) 441
68. D. R. Yarkony, *J. Chem. Phys*. **89** (1988) 7324
69. R. N. Diffenderfer, D. R. Yarkony, *J. Phys. Chem*. **86** (1982) 5098
70. R. N. Diffenderfer, D. R. Yarkony, P. J. Dagdigian, *J. Quant. Spectrosc. Radiat. Transf*. **29** (1983) 329
71. B. Huron, J. P. Malrieu, P. Rancurel, *Chem. Phys*. **3** (1974) 277
72. H. Thümmel, R. Klotz, S. D. Peyerimhoff, *Chem. Phys*. **135** (1989) 229
73. *MOLPRO, version 2008.1, a package of* ab initio *programs*, http://www.molpro.net
74. P. J. Knowles, H.-J. Werner, *Chem. Phys. Lett*. **115** (1985) 259
75. H. J. Werner, P. J. Knowles, *J. Chem. Phys*. **89** (1988) 5803
76. J. Knowles, H.-J. Werner, *Chem. Phys. Lett*. **145** (1988) 514
77. T. H. Dunning, Jr., *J. Chem. Phys*. **90** (1989) 1007
78. D. Feller, *J. Comp. Chem*. **17** (1996) 1571
79. M. Perić, in *Structure and Spectra of Molecules*, M. Gašić, Ed., SASA, Belgrade. 2009 (in Serbian)
80. W. B. White, S. M. Johnson, G. B. Dantzig, *J. Chem. Phys*. **28** (1958) 751
81. J. Radić-Perić, M. Perić, *Spectrochim. Acta, B* **35** (1980) 297
82. J. Radić-Perić, *Spectrochim. Acta, B* **38** (1980) 1021
83. J. Radić-Perić, *Bull. Soc. Chim. Beograd* **49** (1984) 185
84. J. Radić-Perić, *Bull. Soc. Chim. Beograd* **49** (1984) 429
85. J. Radić-Perić, M. Perić, *J. Serb. Chem. Soc*. **50** (1985) 535
86. J. Radić-Perić, *Computers Chem*. **14** (1990) 343
87. J. Radić-Perić, *J. Anal. At. Spectrom*. **7** (1992) 235
88. J. Radić-Perić, J. High Temp. Chem. Processes **2** (1993)115
89. J. Radić-Perić, A. Lađević, *J. Serb. Chem. Soc*. **59** (1993) 491
90. J. Radić-Perić, A. Lađević, *VDI Berichte* **1166** (1995) 487.
91. J. Radić-Perić, M. Markićević, *J. Serb. Chem. Soc*. **65** (2000) 181
92. J. Radić-Perić, N. Pekas, *J. Serb. Chem. Soc*. **66** (2001) 181.
93. J. Radić-Perić, N. Pantelić, *J. Therm. Anal. Cal*. **72** (2003) 35
94. J. Radić-Perić, A. Dašić, *J. Therm. Anal. Cal*. **79** (2005) 59
95. J. Radić-Perić, *Mat. Sci. Forum* **494** (2005) 303
96. J. Radić-Perić, *Mat. Sci. Forum* **518** (2006) 349
97. *JANAF Thermochemical Tables*, Nat. Stand. Ref. Data Ser., US Nat. Bur. Stand. Vol. 27 (1971); *NIST–JANAF Thermochemical Tables, J. Phys. Chem. Ref. Data*, 4th ed., M. W. Chase Jr., Ed., 1999
98. J. Radić-Perić, M. Perić, *Z. Naturforsch.* **42a** (1987) 103
99. J. Radić-Perić, *J. Math. Chem*. **8** (1991) 269
100. M. Perić, J. Radić-Perić, *J. Serb. Chem. Soc*. **60** (1995) 987
101. J. W. Diglee, T. C. Downie, C. W. Goulding, *Chem. Rev*. **69** (1969) 365
102. M. Petković, S. Stojadinović, R. Vasilić, I. Belča, Z. Nedić, B. Kasalica, U. B. Mioč, *Appl. Surf. Sci*. **257** (2011) 9555

2012 Copyright (CC) SCS

103. A. Despic, V. Parkhutik, *Mod. Aspect Electroc*. **20** (1989) 401
104. S. Stojadinovic, Lj. Zekovic, I. Belca, B. Kasalica, D. Nikolic, *Electrochem. Commun*. **6** (2004) 708
105. S. Stojadinovic, I. Belca, B. Kasalica, Lj. Zekovic, M. Tadic, *Electrochem. Commun*. **8** (2006) 1621
106. S. Stojadinovic, M. Tadic, I. Belca, B. Kasalica, Lj. Zekovic, *Electrochim. Acta* **52** (2007) 7166
107. S. Stojadinovic, I. Belca, M. Tadic, B. Kasalica, Z. Nedic, Lj. Zekovic, *J. Electroanal. Chem*. **619–620** (2008) 125
108. S. Stojadinović, R. Vasilić, M. Petković, I. Belča, B. Kasalica, M. Perić, Lj. Zeković, *Electrochim. Acta* **59** (2012) 354
109. S. Stojadinović, R. Vasilić, M. Petković, I. Belča, B. Kasalica, M. Perić, Lj. Zeković, *Electrochim. Acta* **79** (2012) 133
110. S. Ikonopisov, *Electrochim. Acta* **20** (1975) 783
111. S. Stojadinovic, Lj. Zekovic, I. Belca, B. Kasalica, *Electrochem. Commun*. **6** (2004) 427
112. S. Stojadinovic, I. Belca, Lj. Zekovic, B. Kasalica, D. Nikolic, *Electrochem. Commun*. **6** (2004) 1016
113. B. Kasalica, S. Stojadinovic, Lj. Zekovic, I. Belca, D. Nikolic, *Electrochem. Commun*. **6** (2005) 735
114. B. Kasalica, I. Belca, S. Stojadinovic, M. Sarvan, M. Peric, Lj. Zekovic, *J. Phys. Chem., C* **111** (2007) 12315
115. M. Sarvan**,** S. Stojadinovic, B. Kasalica, I. Belca, Lj. Zekovic, *Electrochim. Acta* **53** (2008) 2183
116. S. Stojadinovic, R. Vasilic, I. Belca, M. Tadic, B. Kasalica, Lj. Zekovic, *Appl. Surf. Sci*. **255** (2008) 2845
117. S. Stojadinovic, R. Vasilic, M. Petkovic, Z. Nedic, B. Kasalica, I. Belca, Lj. Zekovic, *Electrochim. Acta* **55** (2010) 3857
118. M. Sarvan, M. Perić, Lj. Zeković, S. Stojadinović, I. Belča, M. Petković, B. Kasalica, *Spectrochim. Acta A* **81** (2011) 672
119. S. Stojadinovic, R. Vasilic, I. Belca, M. Petkovic, B. Kasalica, Z. Nedic, Lj. Zekovic, *Corros. Sci*. **52** (2010) 3258
120. M. Petković, S. Stojadinović, R. Vasilić, Lj. Zeković, *Appl. Surf. Sci*. 257 (2011) 10590
121. M. D. Klapkiv, H. M. Nykyforchyn, V. M. Posuvailo, *Mater. Sci*. **30** (1994) 333
122. C. S. Dunleavy, I. O. Golosnoy, J. A. Curran, T. W. Clyne, *Surf. Coat. Technol*. **203** (2009) 3410
123. J. Jovović, S. Stojadinović, N. M. Šišović, N. Konjević, *J. Quant. Spectrosc. Radiat. Transfer* **113** (2012) 1928
124. R. O. Hussein, X. Nie, D. O. Northwood, A. Yerokhin, A. Matthews, *J. Phys., D* **43** (2010) 105203
125. S. Stojadinović, J. Jovović, M. Petković, R. Vasilić, N. Konjević, *Surf. Coat. Technol*. **205** (2011) 5406
126. J. Jovović, S. Stojadinović, N. M. Šišović, N. Konjević, *Surf. Coat. Technol*. **206** (2011) 24
127. S. Stojadinović, R. Vasilić, M. Petković, Lj. Zeković, *Surf. Coat. Technol*. **206** (2011) 575
128. R. O. Hussein, P. Zhang, X. Nie, Y. Xia, D. O. Northwood, *Surf. Coat. Technol*. **206** (2011) 1990

2012 Copyright (CC) SCS

129. S. Stojadinović. M. Perić, M. Petković, R. Vasilić, B. Kasalica, I. Belča, J. Radić-Perić, *Electrochim. Acta* **56** (2011) 10122
130. S. Stojadinović, R. Vasilić, M. Petković, I. Belča, B. Kasalica, M. Perić, Lj. Zeković, *Electrochim. Acta* **59** (2012) 354
131. S. Stojadinović, M. Perić, J. Radić-Perić, R. Vasilić, M. Petković, Lj. Zeković, *Surf. Coat. Technol*. **206** (2012) 2905
132. R. O. Hussein, X. Nie, D. O. Northwood, *Mater. Phys. Chem.* **134** (2012) 484
133. B. V. Kasalica, I. D. Belca, S. Đ. Stojadinovic, Lj. D. Zekovic, D. Nikolic, *Appl. Spectrosc*. **60** (2006) 1090
134. H. Chen, G. H. Lv, G. L. Zhang, H. Pang, X. Q. Wang, H. J. Lee, S. Z. Yang, *Surf. Coat. Technol*. **205** (2010) S32
135. J. Cai, F. Caoa, L. Chang, J. Zheng, J. Zhang, C. Cao, *Appl. Surf. Sci*. **257** (2011) 3804
136. L. Zhao, C. Cui, Q. Wang, S. Bu, *Corr. Sci*. **52** (2010) 2228
137. A. Bai, *Surf. Coat. Technol*. **204** (2010)1856
138. J. Liang, P. Bala Srinivasan, C. Blawert, W. Dietzel, *Electrochim. Acta* **55** (2010) 6802
139. R. Arrabal, E, Matykina, T. Hashimoto, P. Skeldon, G. E. Thompson, *Surf. Coat. Technol*. **203** (2009) 2207
140. R. O. Hussein, P. Zhang, D. O. Northwood, X. Nie, *Corros. Mater*. **36** (2011) 38
141. Yu. Ralchenko, A.E. Kramida, J. Reader and NIST ASD Team (2011), NIST Atomic Spectra Database (ver. 4.l.0) [Online], National Institute of Standards and Technology, Gaithersburg, MD
142. C. de Izarra C, *J. Phys. D*: *Appl. Phys*. **33** (2000) 1697
143. M. Klapkiv, *Mater. Sci*. **31** (1995) 394
144. M. Klapkiv, *Mater. Sci*. **35** (1999) 279
145. A. L. Yerokhin, X. Nie, A. Leyland, A. Matthews, S. J. Dowey, *Surf. Coat. Technol.* **122** (1999) 73.

2012 Copyright (CC) SCS